Day 2: Measurement of weak continued

From pixels to cosmology

Photometric calibration.
Astrometric calibration.
Dithering.
Masking.
PSF systematics continued.
Shear bias continued.
Shear calibration continued.

Galaxy-galaxy lensing

Photometric calibration I

- Most important for photometric redshifts
- Variation in photometric zero-point → variation in galaxy number, noise → selection biases
- Wide-field surveys accurate to sub-% magnitudes

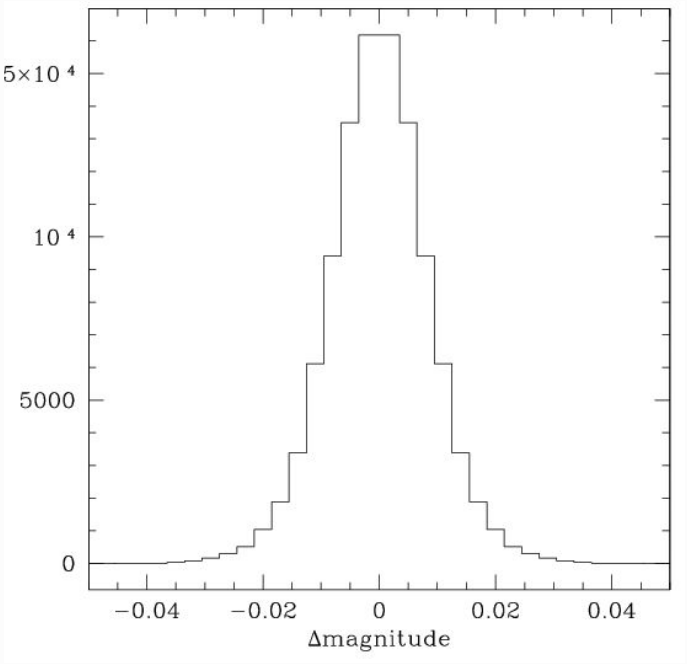

CFIS − Pan-STARRS r-band magnitude differences.
[From Stephen Gwyn]

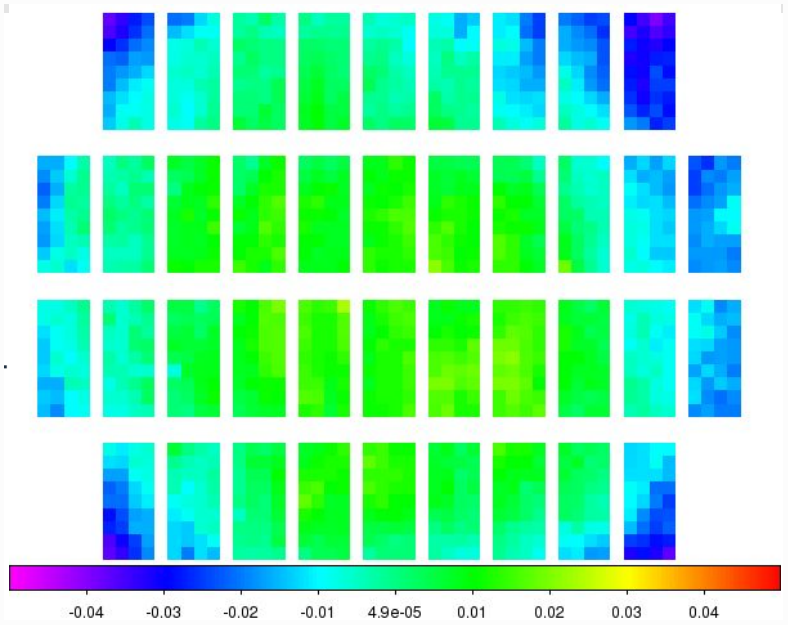

CFIS r-band magnitude correction across focal plane.

Photometric calibration II

CFIS vs. Pan-STARRS r-band magnitude differences

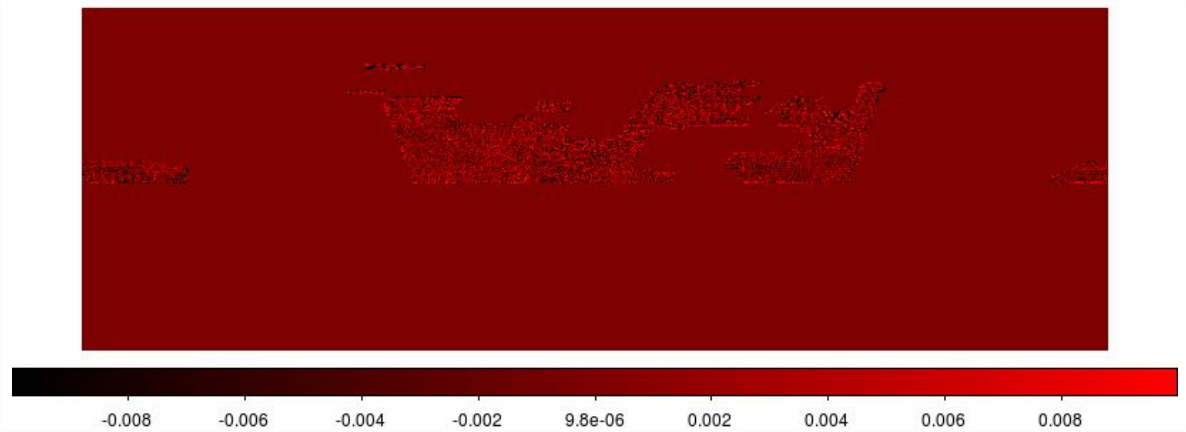

CFIS vs. SDSS r-band magnitude differences

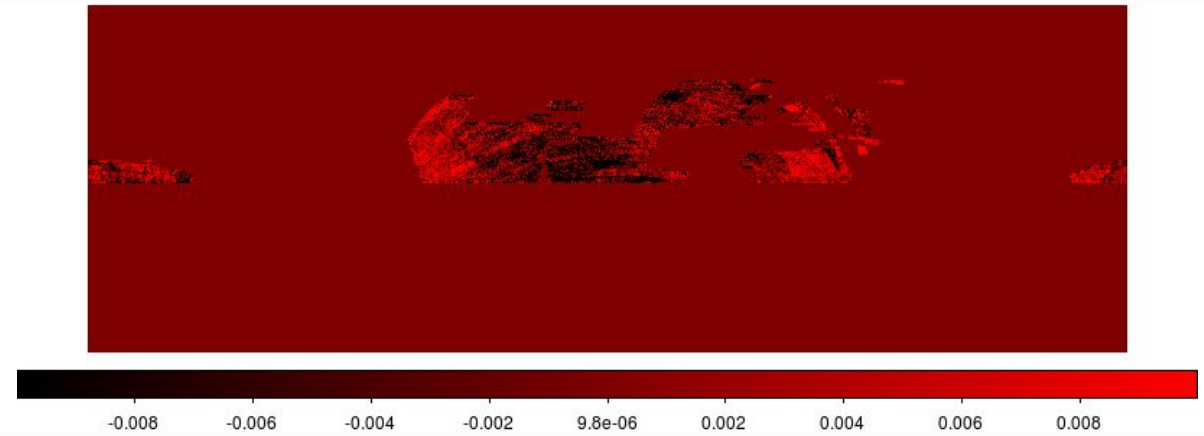

Astrometric calibration

- Crucial for weak lensing.
- Errors in astrometry can induce
  - (additive) shear biases
  - E- and B-mode mixing
  - shape measurement errors from (incorrectly) co-added exposures (relative astrometric accuracy between exposures)
- Typically much better than telescope pointing accuracy
- Image distortions are fit with function, e.g. 2D polynomial, to reference (star) sample
- Best fit is called "astrometric solution"
- In last years use GAIA catalogue for absolute reference, increased accuracy by order of magnitude, to ~ 20 mas
- Need to account for higher-order effects e.g. differential chromatic refraction (DCR), stellar proper motions

Dithering

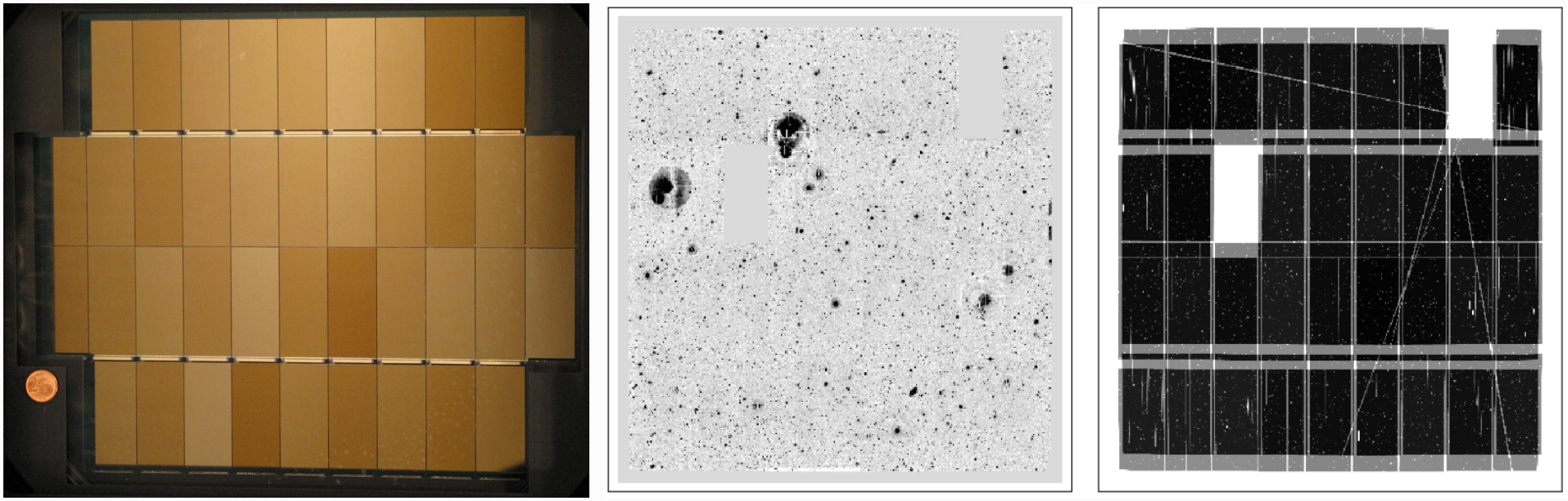

Left: Image of the MegaCam focal plane (CCDs arrays).
Middle: Co-add of two r-band exposures of CFHTLenS (without the 4 new CCDs).
Right: Weight map.

Stacking methods:

- median: removes most outliers (e.g. cosmic rays, satellite tracks)
- (weighted) mean: linear operation, leads to simple stacked PSF (also weighted mean of single-exposure PSFs)

Dithering: large dithers

Some surveys (DES, CFIS) have large dithers, which is better for photometric homogeneity. *However*, the PSF of the co-added (stacked) image likely to be complex and discontinuous.

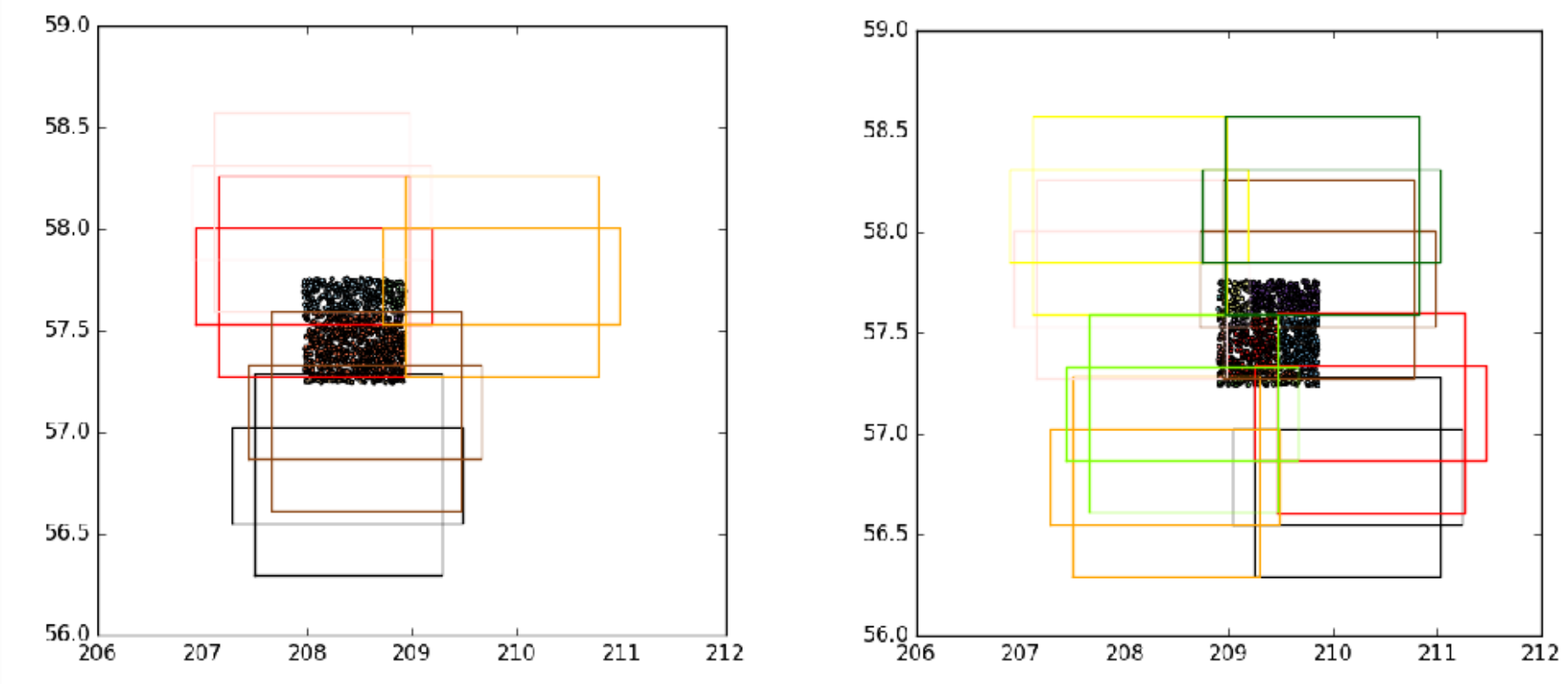

CFIS dithering.

[From Morgan Schmitz].

Masking

Need to mask:

- Areas of bad or uncalibrated photometry:
  bad or saturated pixels, sometimes chip borders, halos of bright stars
- artefacts that can be mis-classified as lensing galaxies:
  cosmic rays, satellite tracks, asteroids, bright stars with their halos and diffraction spikes, nearby galaxies with substructure (e.g. globular clusters, star-forming regions)

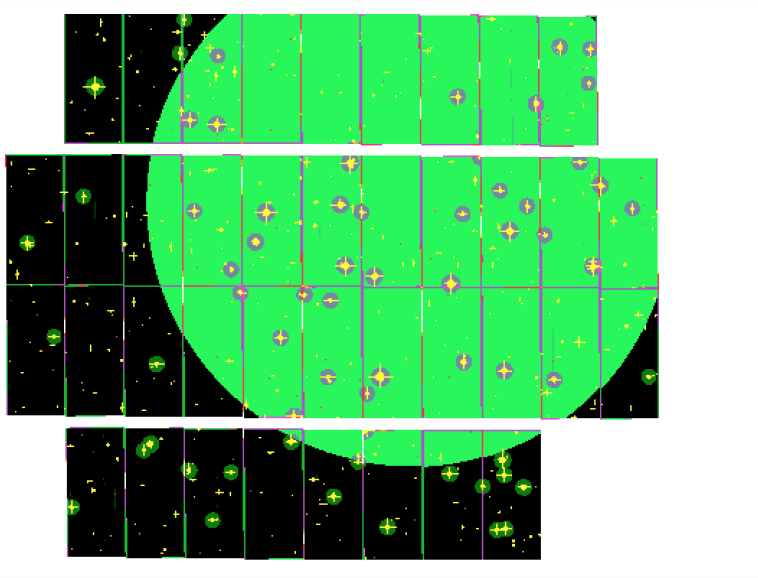

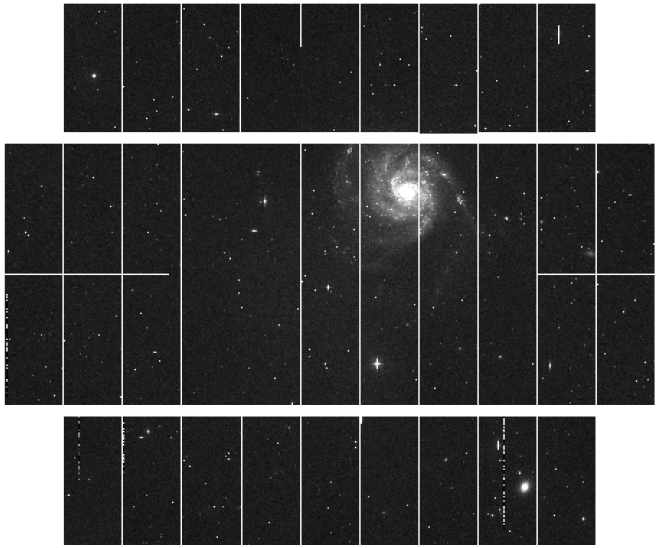

Quantifying PSF systematics: residuals

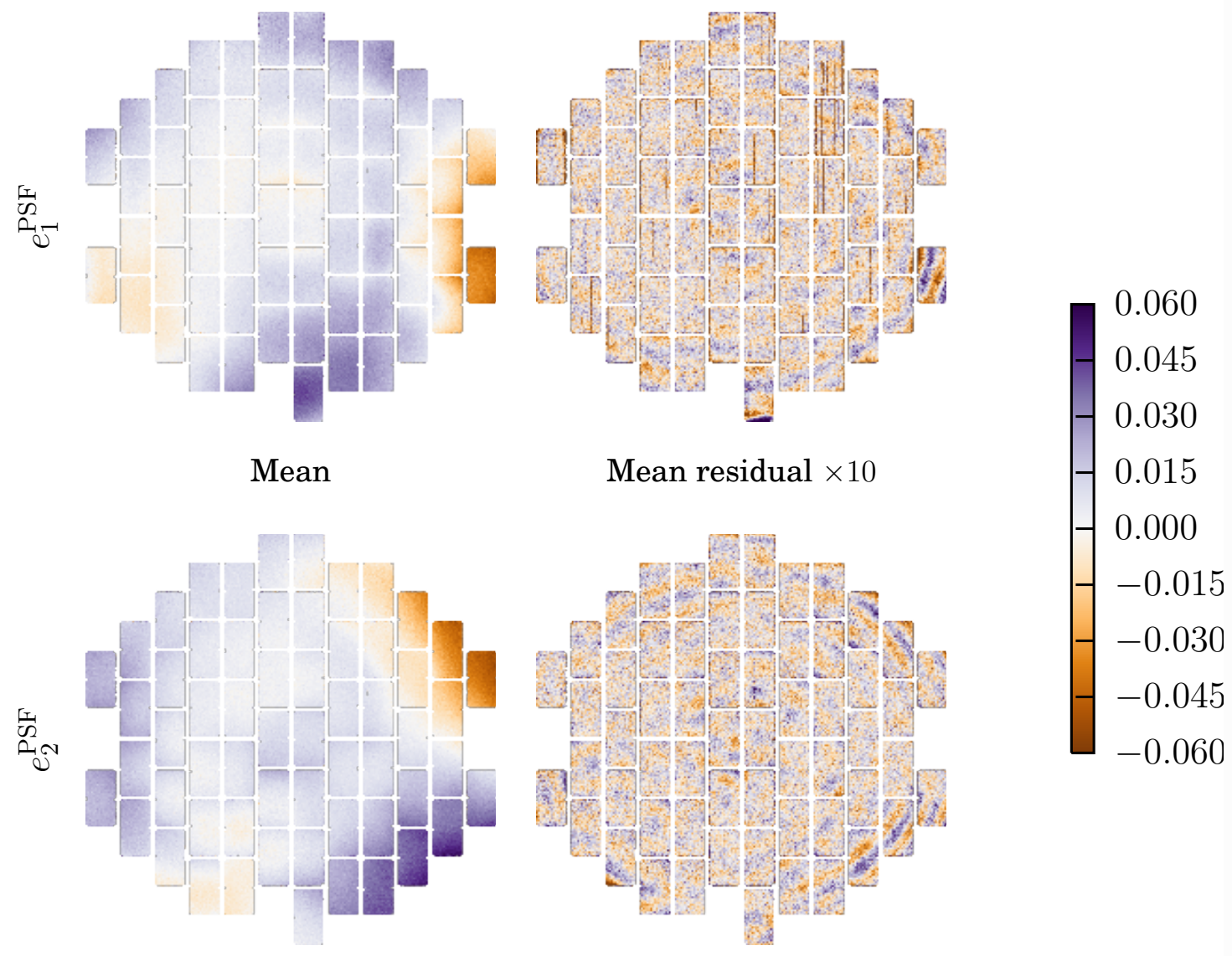

DES-Y1, (Zuntz et al. 2018)

Quantifying PSF systematics: residuals

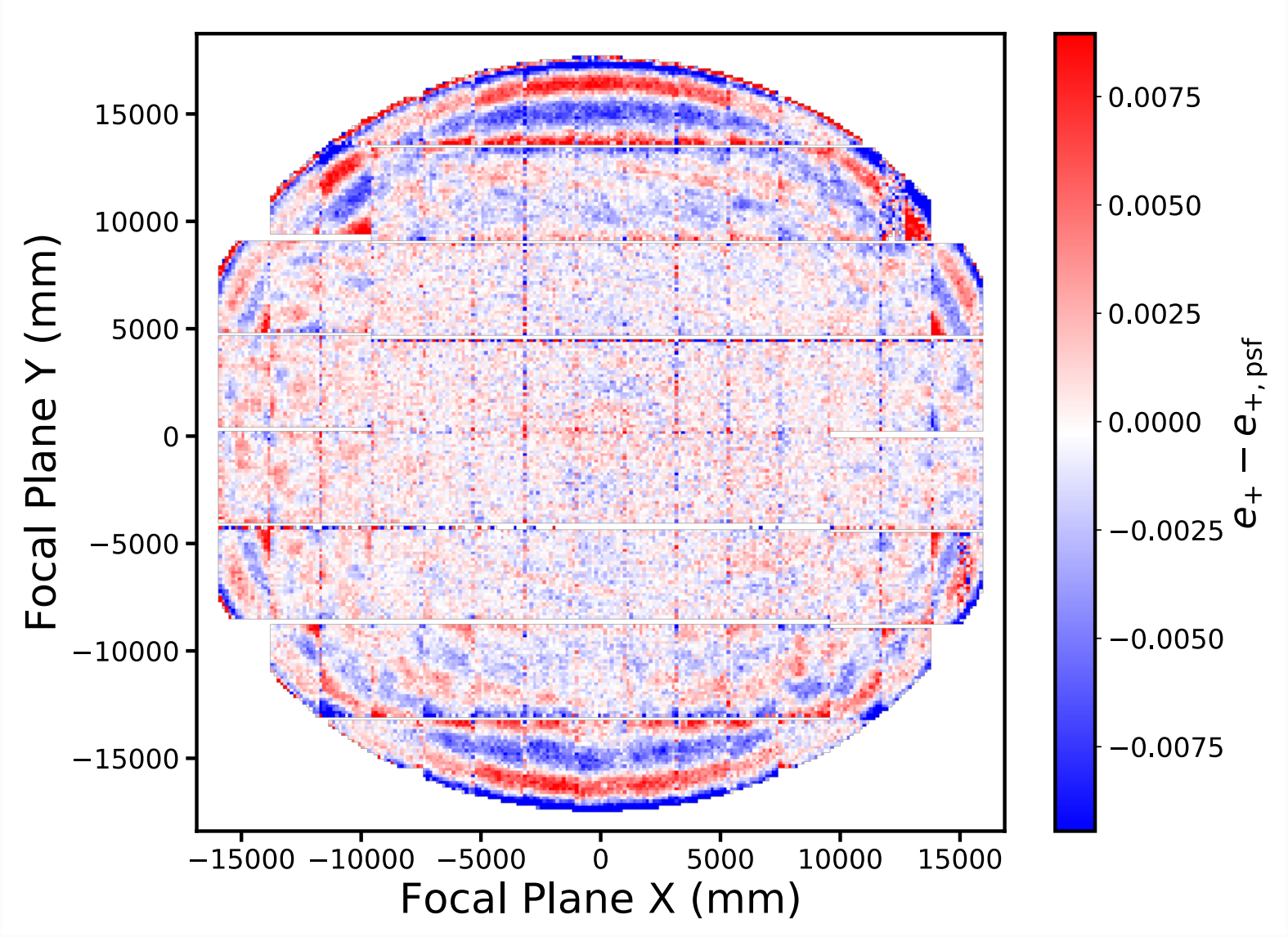

HSC, (Mandelbaum 2018)

Quantifying PSF systematics: residuals

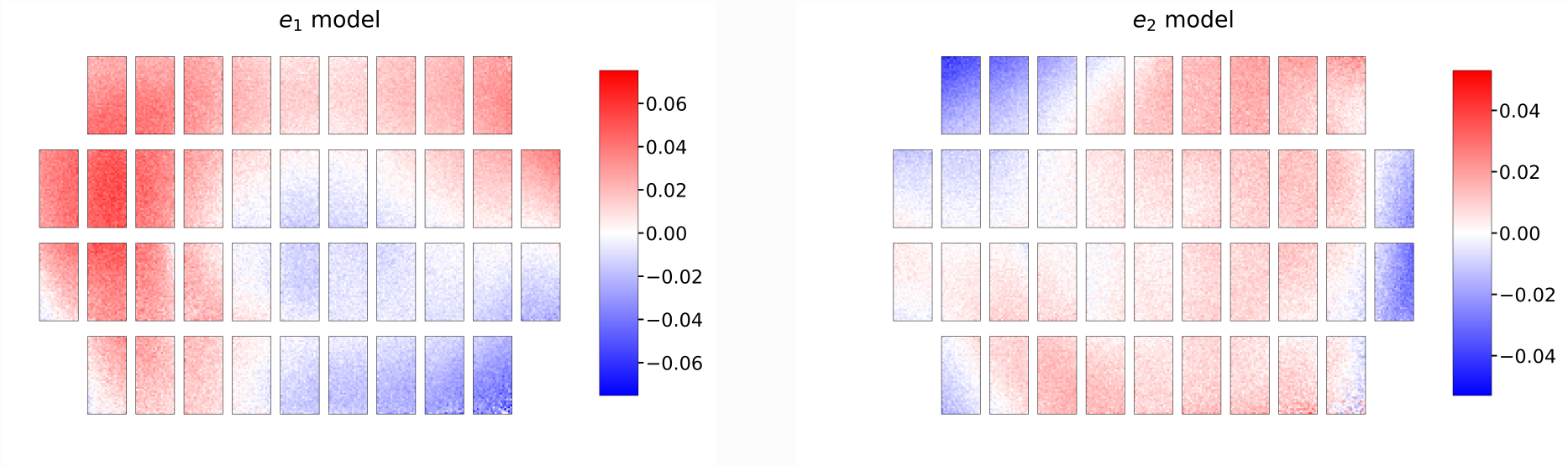

CFIS, (Guinot et al. 2021).

Shear bias

Reminder: Write as multiplicative and additive bias:

$$\langle \varepsilon_\alpha^{\rm obs} \rangle = g_\alpha^{\rm obs} = (1 + m_\alpha) g_\alpha^{\rm true} + c_\alpha; \quad \alpha = 1, 2.$$

There is also ellipticity bias, which is different:

$$\varepsilon_i^{\rm obs} = (1 + m_i') \varepsilon_i^{\rm true} + c_i'; \quad i = 1, 2.$$

Typical values:

year	program	Δm	Δc	$\sigma(c)$
2006	STEP I	0.1		10^{-3}
2012	CFHTLenS	0.06	0.002	
2013	great3	0.01	10^{-3}	
2014	DES	0.03–0.04	10^{-3}	
2016	KiDS	0.01–0.02	$8 \cdot 10^{-4}$	
2021	Euclid required	$2 \cdot 10^{-3}$	$5 \cdot 10^{-4}$	

Shear bias and simulations I

From the STEP I shear measurement challenge (Heymans et al. 2006).

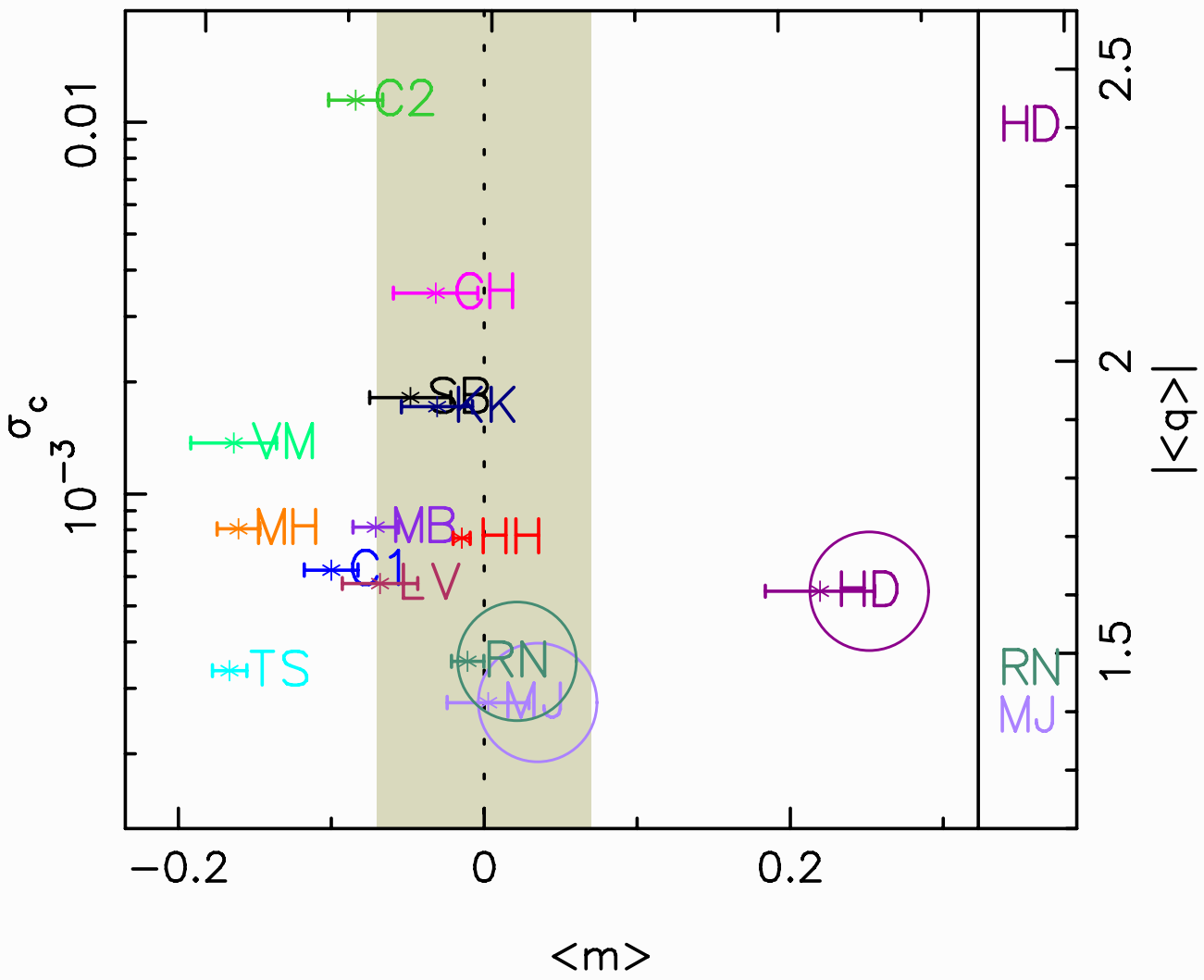

Shear bias and simulations II

From the great3 shear measurement challenge (Mandelbaum et al. 2015).

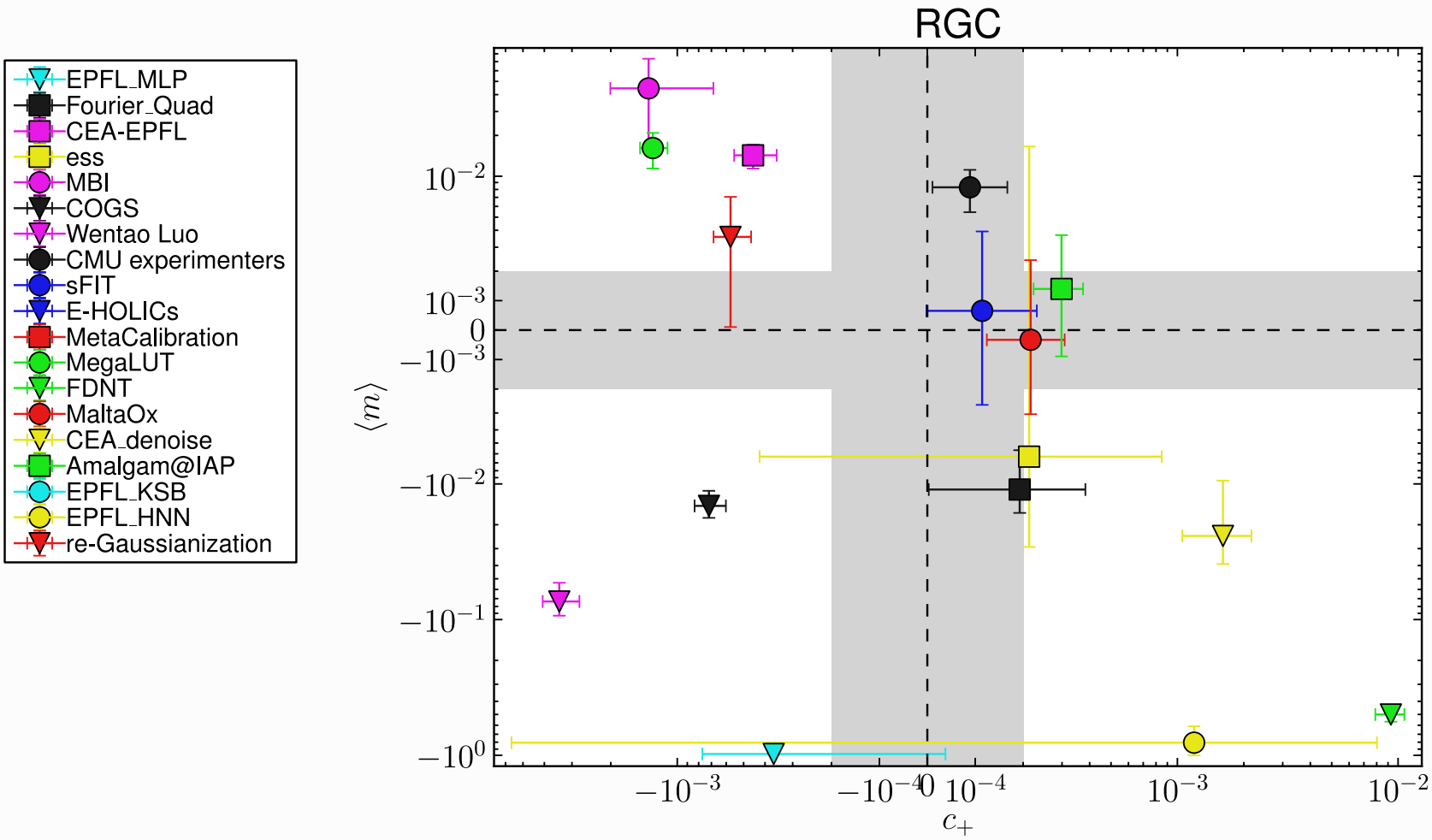

Shear bias and simulations III

Interpret with caution!

- Small biases because simulations are not realistic enough? E.g. constant PSF, analytical galaxy light distributions, simplistic noise, (constant shear)
- Simulation (challenges) only address part of the problem. Usually no blended galaxy images, star-galaxy separation, color effects, ...
- Calibrated or un-calibrated?

Amplitude of m, c not that important, since they can be calibrated empirically. What counts are $\Delta m, \Delta c$ after calibration!

More on this in a few slides.

Shear bias and simulations IV

A very general statement (see Part I day 2):

Most ellipticity estimators are non-linear pixel light distribution. Noise then creates biases in the estimator. This is called noise bias.

Thus, observed shear needs to be de-biased (calibrated) using simulations.

There are a few unbiased estimators:

- Not normalised to total flux: maybe unbiased, but very large variance
- Bayesian estimators, sample posterior distribution, unbiased if correct model, likelihood and prior.
  Prior needs to be estimated from simulations or deep survey!

Shear calibration

The bias should be *robust* for method to be *calibratable* using image simulations.
Define *sensitivity* as dependence of bias with respect to parameters, or

$$|\partial m/\partial p_i|, \quad \text{for } \boldsymbol{p} = \text{set of parameters.}$$

A method is calibratable from simulations, see (Hoekstra et al. 2017), if

- the sensitivity is small (otherwise simulation sampling in p too costly)
- does not depend on too many parameters
- those parameters can be measured accurately (e.g. intrinsic ellipticity dispersion σ_ε from Euclid Deep Survey $\rightarrow$ requirement on accuracy of measured σ_ε sets area of calibration fields)
- those parameters can be reasonably simulated to estimate sensitivity
- difficult if parameter is correlted with shear signal (e.g. local galaxy density with large-scale structure, correlated with shear signal, magnification)

Sources of bias

Reminder:

- Noise bias
- Model bias
  - Model-fitting method: incorrect model, complex galaxy morphology
  - Direct estimation: inappropriate filter function for weighted moments; truncated eigenfunction decomposition
  - Ellipticity gradients
  - Color gradients
- PSF residuals
- CTI (charge transfer inefficiency)
- Selection effects (population biases). Detection probability depends on ellipticity, orientation with PSF, pixel scale
- New: Environmental effects
  - Unresolved faint galaxies

Shear calibration: Unresolved faint galaxies I

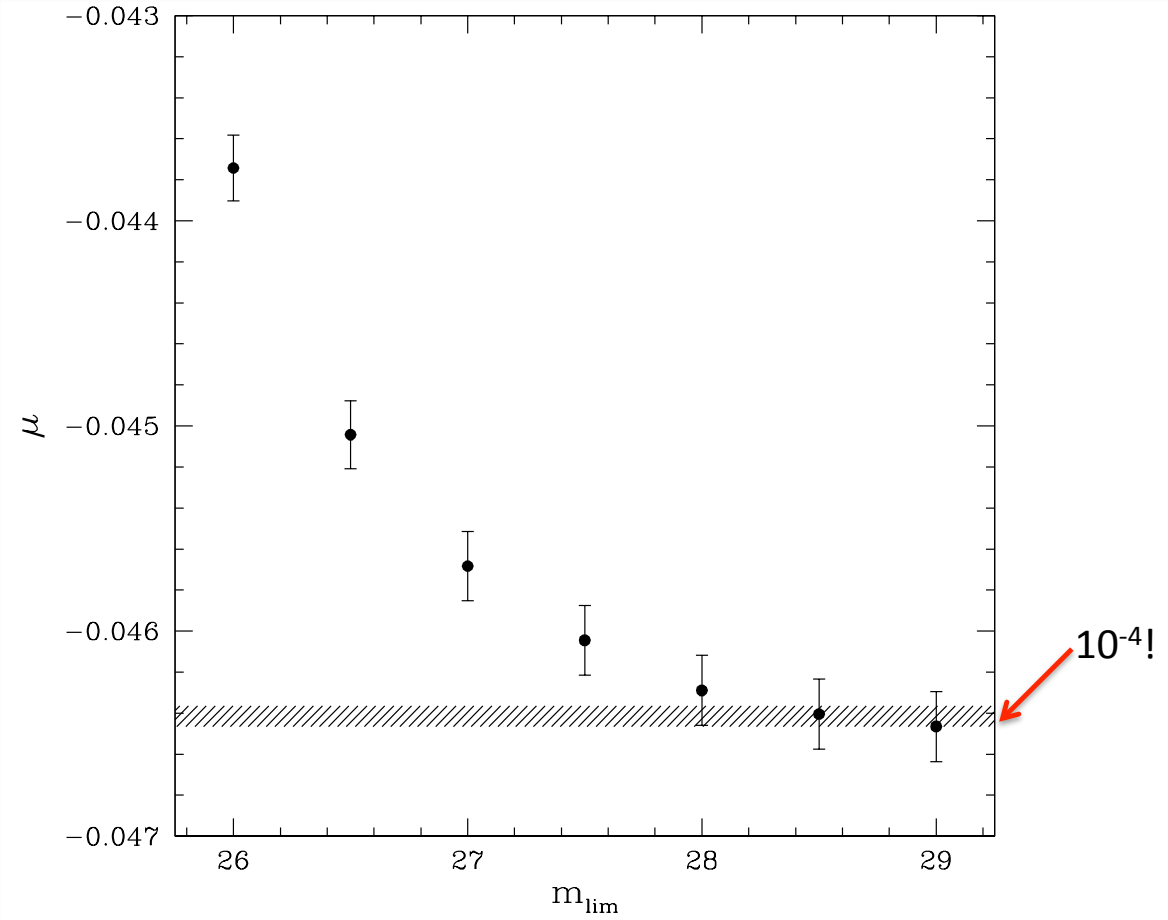

Multiplicative bias m (here μ) for galaxies $20 < m < 24.5$ as function of limiting magnitude of simulated galaxies. From (Hoekstra et al. 2017).

Overall values on y-axis (amplitude of m) not really important, will be corrected for.

Need simulation up to very high depth, until plateau in m is reached ($\partial m / \partial m_{\rm lim} = 0$).

Error bars need to decrease to match hashed region.

Shear calibration: Unresolved faint galaxies II

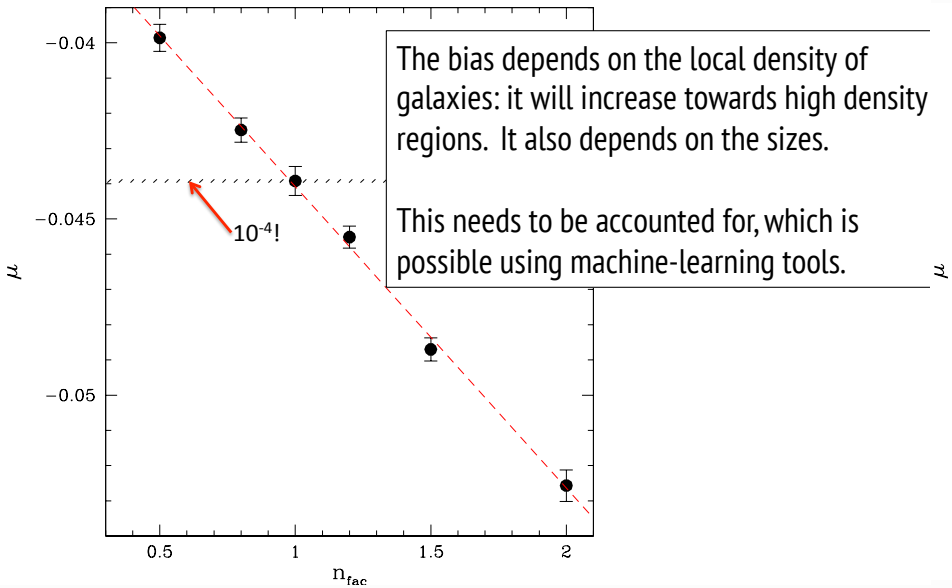

The bias depends on the local density of galaxies: it will increase towards high density regions. It also depends on the sizes.

This needs to be accounted for, which is possible using machine-learning tools.

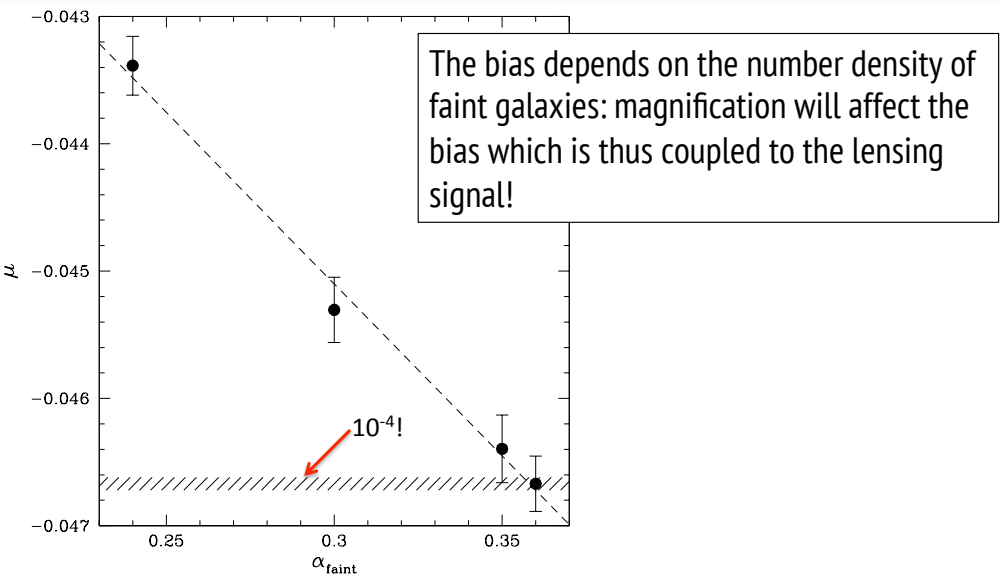

The bias depends on the number density of faint galaxies: magnification will affect the bias which is thus coupled to the lensing signal!

(Hoekstra et al. 2017)

Shear calibration from simulations: tricks of the trade I

Again: multiplicative and additive bias,

$$\langle \varepsilon_\alpha^{\rm obs} \rangle = g_\alpha^{\rm obs} = (1+m_\alpha) g_\alpha^{\rm true} + c_\alpha; \quad \alpha = 1,2.$$

for sample of galaxies with vanishing intrinsic ellipticity $\langle \varepsilon_\alpha^{\rm I} \rangle = 0$.
How can we determine the multiplicative bias from image simulations?

Simple method

From linear fit of many simulated pairs $(\varepsilon_\alpha^{\rm obs}, g_\alpha^{\rm true})$.

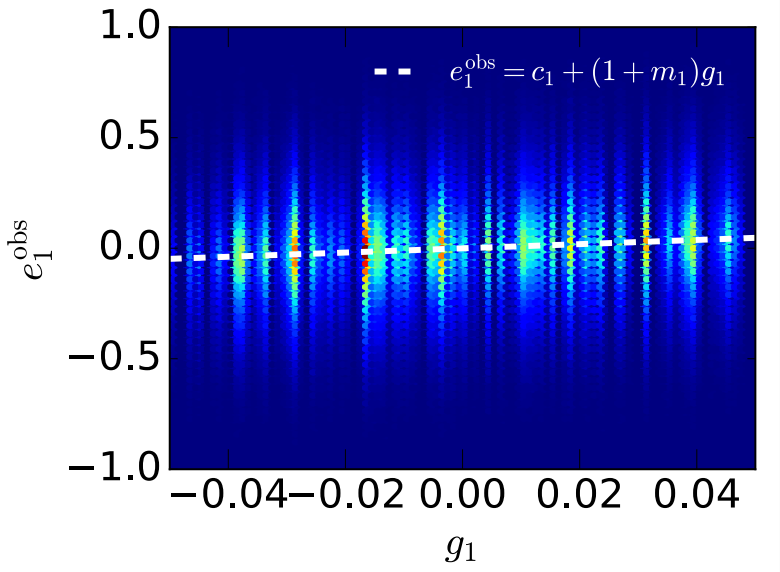

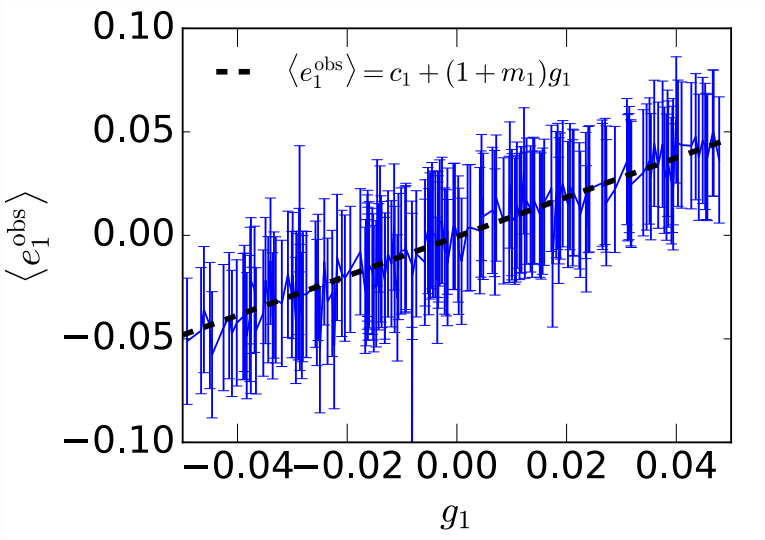

Shear calibration from simulations: tricks of the trade II

Error on best-fit m_α given by width in $\varepsilon^{\rm obs}$ (including measurement errors), $g^{\rm true}$, and stochasticity of galaxy images (from pixel noise),

$$\sigma_{m,\alpha} = \frac{1}{\sqrt{N}} \sqrt{\sigma^2_{R,\alpha} + \frac{\sigma^2_{S,\alpha}}{\sigma^2_{g,\alpha}}}; \quad S = f(\varepsilon^{\rm I}).$$

Second terms is dominant in most cases.

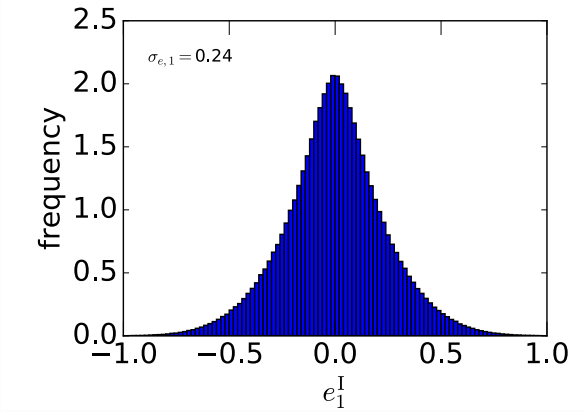

Ell. distribution.

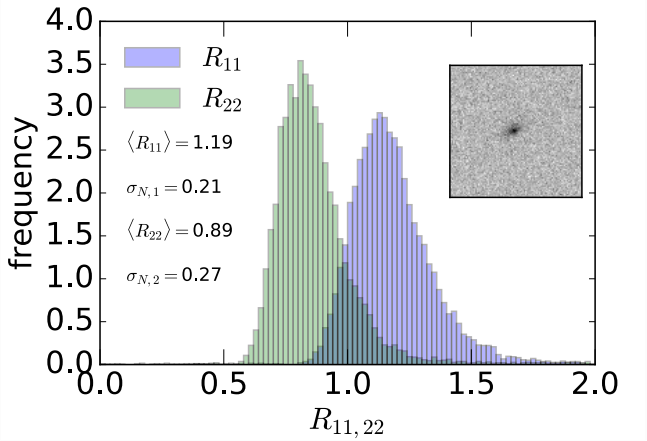

Stochasticity for low SNR.

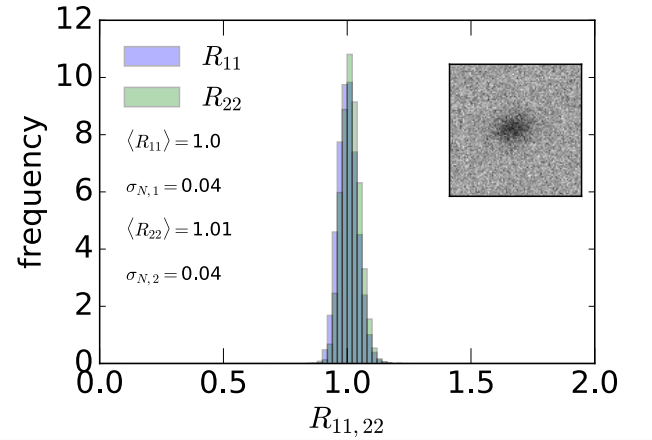

Stochasticity for high SNR.

Shear calibration from simulations: tricks of the trade III

Noise suppression

Simulate pairs of galaxies with same shear and orthogonal intrinsic ellipticity (rotated by 90 degrees),

$$\varepsilon_A^{\mathrm{I}} + \varepsilon_B^{\mathrm{I}} = 0.$$

This however does not mean that the *observed* ellipticity vanishes, due to:

- Measurement stochasticicy
- Ellipticity bias, if depends on galaxy orientation wrt PSF, shear, (pixelization)
- Selection effects, one pair member might drop out of sample

Shear calibration from simulations: tricks of the trade IV

More advanced noise suppression: ring test. Simulate n galaxies with equidistant intrinsic ellipticity on ring around 0.

Derivative method

As seen yesterday, write shear bias for individual galaxies, and as matrix equation (Huff & Mandelbaum 2017):

$$\boldsymbol{\varepsilon}_\alpha^{\mathrm{obs}} = \mathbf{R}\boldsymbol{g}^{\mathrm{true}} + \boldsymbol{c}$$

To get population bias, average over measured shear responses $\langle R \rangle$, and correct measured ellipticities by $\langle R \rangle^{-1}$.

Measure individual $\mathbf{R}$ as numerical derivatives

$$R_{\alpha\beta} = \frac{\partial \varepsilon_\alpha^{\mathrm{obs}}}{\partial g_\beta}$$

by simulating the same galaxy several times with small added shear.

With same noise realisation this measurement is extremely precise!

Shear calibration from simulations: tricks of the trade V

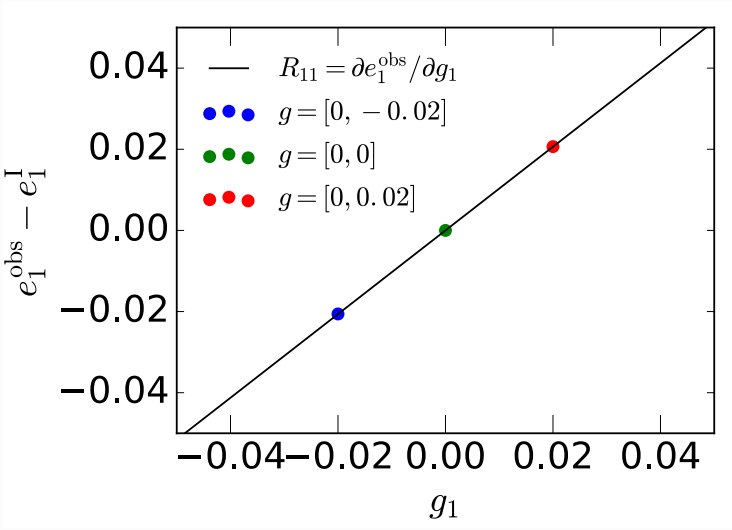

This measurement is independent of ellipticity (observed and intrinsic) and thus removes the main uncertainty of error!
Note: For a different noise realisation, the obtained $\mathbf{R}$ can be quite different. But the use of many simulated galaxy images assures the sampling of the distribution of R, no additional error is introduced on the population bias.
Error on bias estimate:

$$\sigma_{m,\alpha} = \frac{\sigma_{R,\alpha}}{\sqrt{N}}$$

This method requires a factor of several hundred fewer image simulations.

Shear calibration from simulations: tricks of the trade VI

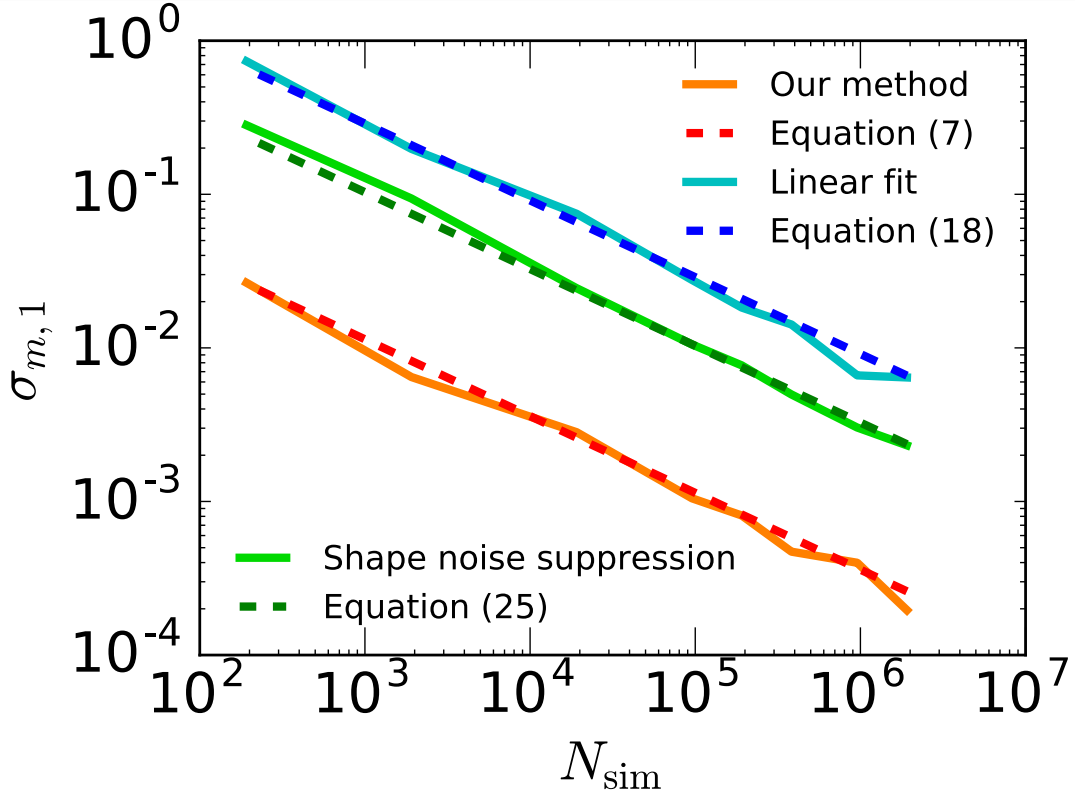

From (Pujol et al. 2019).

Shear calibration from deep learning I

Train neural network to learn (via linear regression) shear bias as function of observed galaxy (and PSF) properties.
NN automatically finds most relevant input quantities to predict shear bias.
Using trained network (model), use real data as input to estimate shear bias.

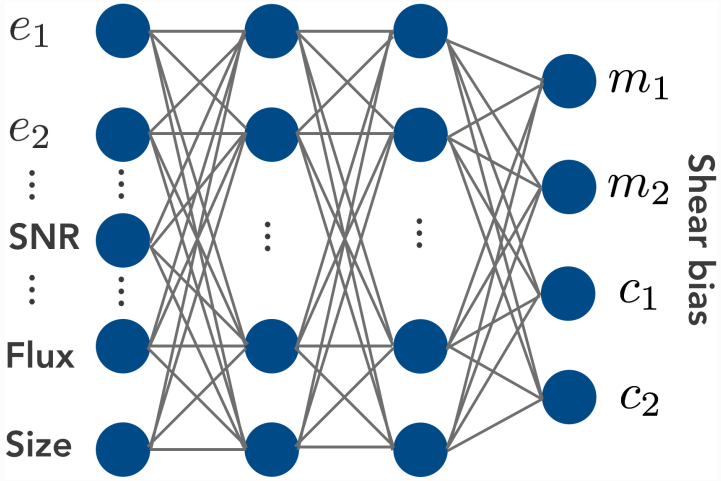

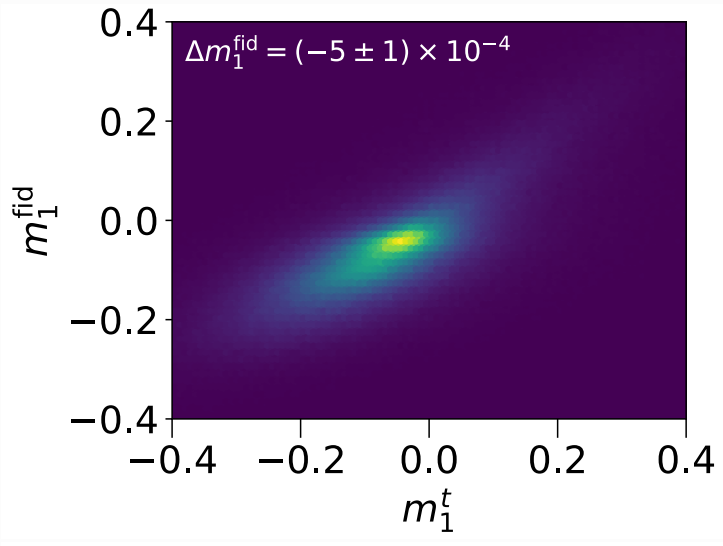

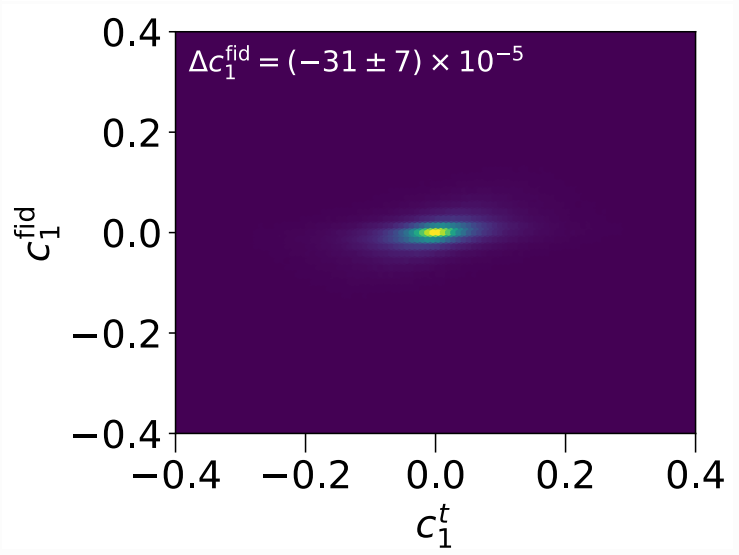

(Pujol et al. 2020)

Shear calibration from deep learning II

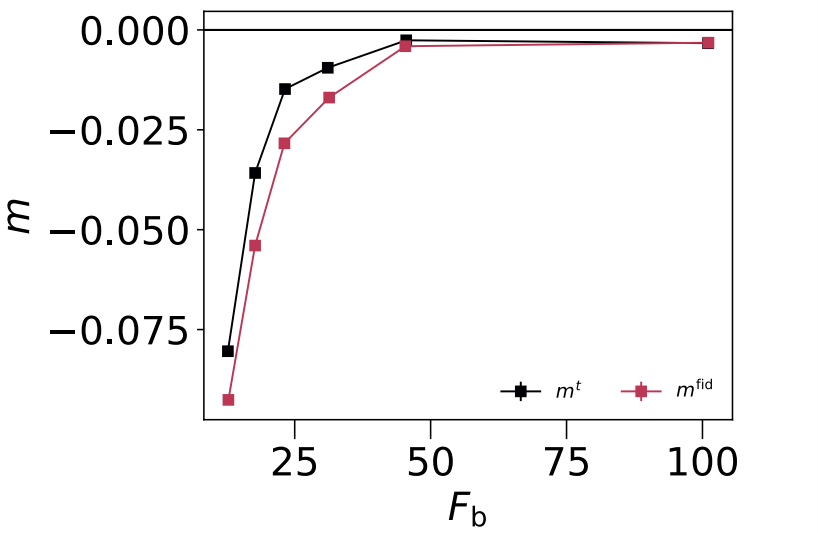

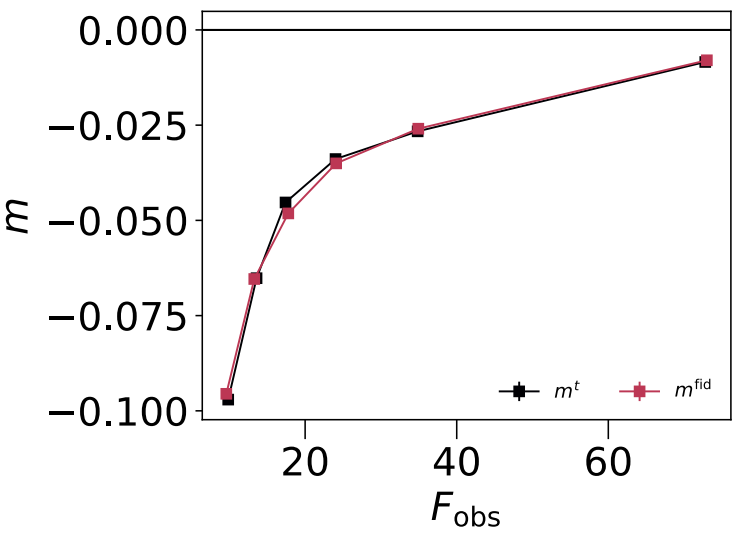

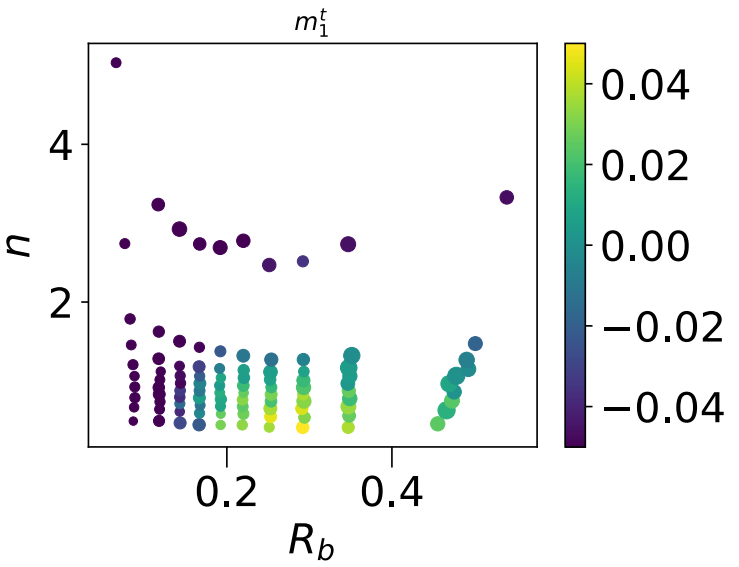

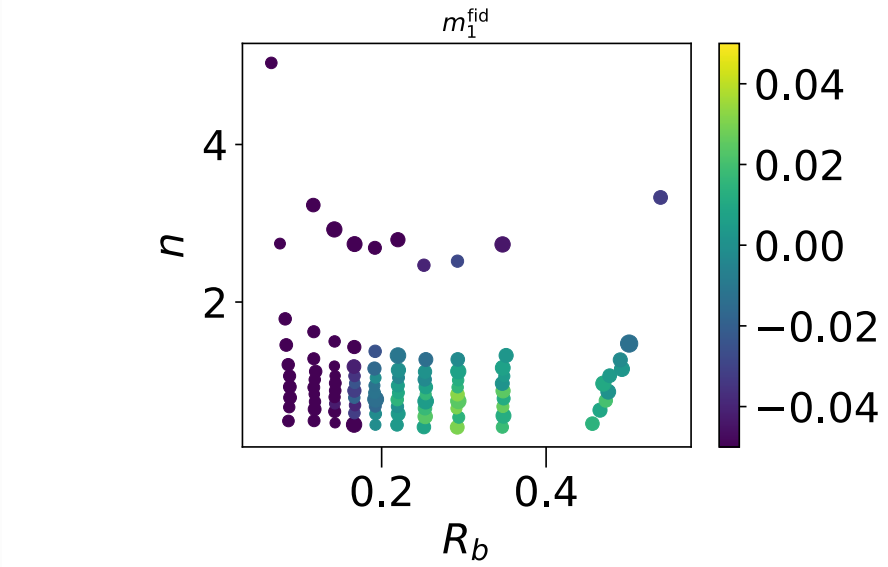

(Pujol et al. 2020)

E- and B-modes: recap from cycle 1

Shear patterns

We have seen tangential pattern in the shear field due to mass over-densities.
Under-dense regions cause a similar pattern, but with opposite sign for γ.
That results in radial pattern.

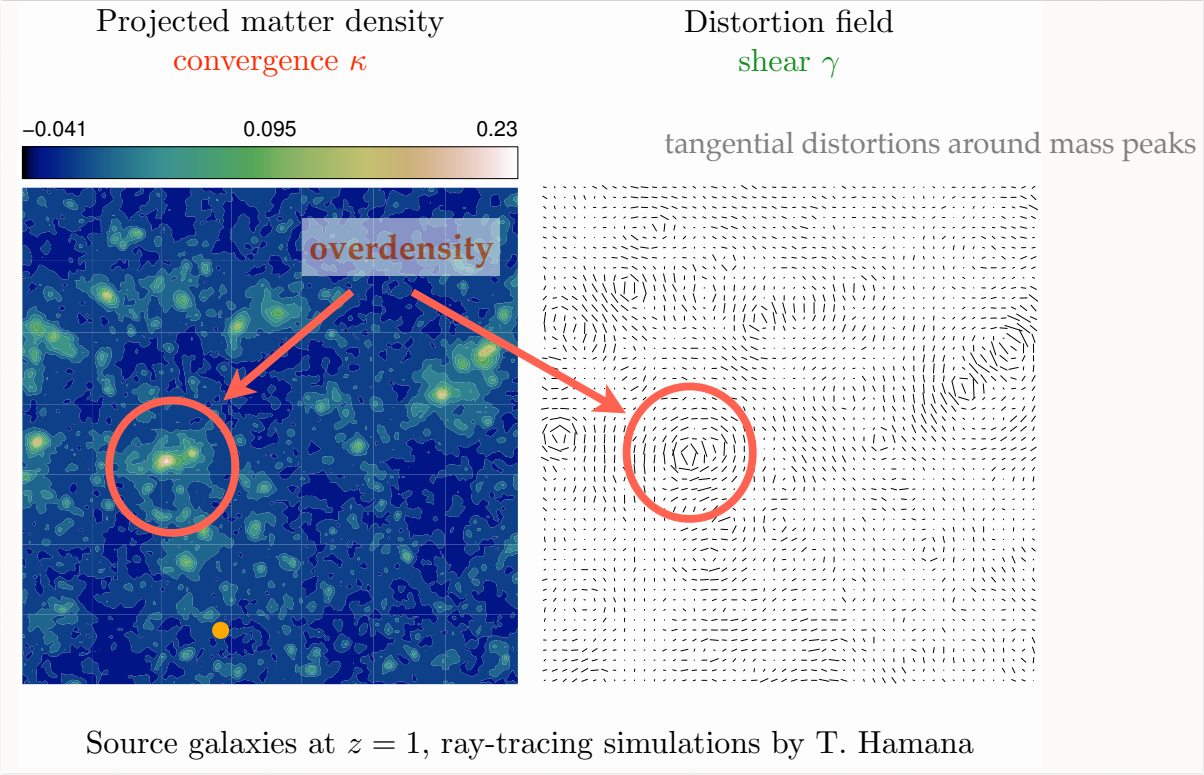

Source galaxies at $z = 1$, ray-tracing simulations by T. Hamana

E- and B-modes: recap from cycle 1

Shear patterns

We have seen tangential pattern in the shear field due to mass over-densities. Under-dense regions cause a similar pattern, but with opposite sign for γ. That results in radial pattern.

Under idealistic conditions, these are the only possible patterns for a shear field, the E-mode. A so-called B-mode is not generated.

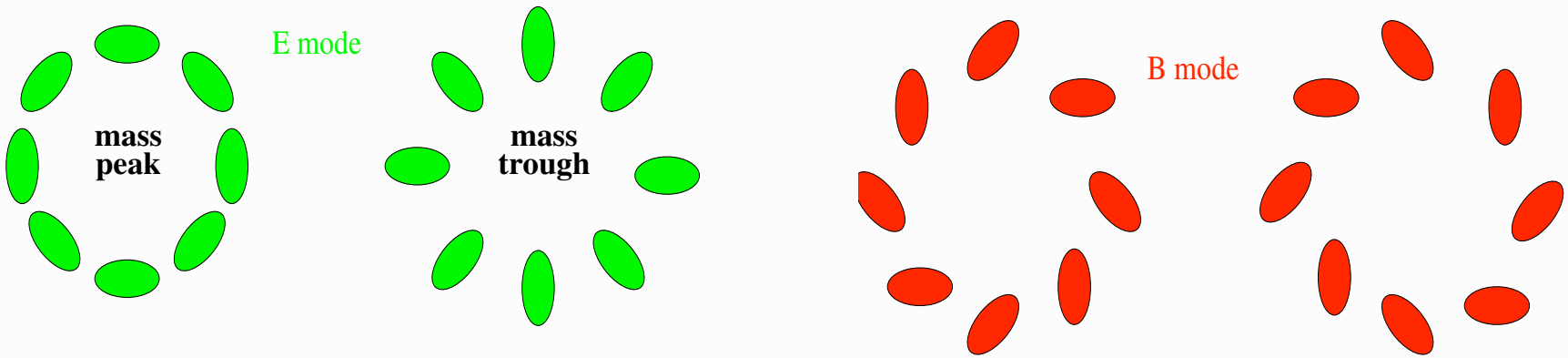

Tangential shear and surface mass I

What is the actual relationship between tangential shear and projected surface mass?
It can be shown that the tangential shear around a mass concentration at angular distance θ *only* depends on the encompassed projected surface mass, minus a boundary term:

$$\langle \gamma_{\rm t} \rangle (\theta) = \bar{\kappa}(\leq \theta) - \langle \kappa \rangle (\theta).$$

We will re-write equation defining the *surface mass excess* $\Delta\Sigma$.

Before that: brief reminder of relation between lensing convergence and matter density from last year.

Reminder: Convergence and cosmic density contrast

Back to the lensing potential

- Since $\kappa = \frac{1}{2}\Delta\psi$:

$$\kappa(\boldsymbol{\theta}, \chi) = \frac{1}{c^2}\int_0^\chi \mathrm{d}\chi' \frac{(\chi - \chi')\chi'}{\chi} \Delta_{\boldsymbol{\theta}}\phi(\chi'\boldsymbol{\theta}, \chi')$$

- Terms $\Delta_{\chi'\chi'}\phi$ average out when integrating along line of sight, can be added to yield 3D Laplacian (error $\mathcal{O}(\phi) \sim 10^{-5}$).
- Poisson equation

$$\Delta\phi = \frac{3H_0^2\Omega_\mathrm{m}}{2a}\,\delta \qquad \left(\delta = \frac{\rho - \bar{\rho}}{\rho}\right)$$

$$\rightarrow \kappa(\boldsymbol{\theta}, \chi) = \frac{3}{2}\Omega_\mathrm{m}\left(\frac{H_0}{c}\right)^2 \int_0^\chi \mathrm{d}\chi' \frac{(\chi - \chi')\chi'}{\chi a(\chi')}\,\delta\left(\chi'\boldsymbol{\theta}, \chi'\right).$$

Tangential shear and surface mass I

Going back to the equation betwene tangential shear and encompassed projected surface mass,

$$\langle \gamma_{\rm t} \rangle (\theta) = \bar{\kappa}(\leq \theta) - \langle \kappa \rangle (\theta).$$

Now we are ready to re-write equation defining the *surface mass excess* $\Delta\Sigma$.

Surface mass excess

Assume a single lens at (angular diameter) distance $D_{\rm l}$. Approximate for this case the expression of the convergence

$$\kappa(\boldsymbol{\theta}, \chi) = \frac{3}{2}\Omega_{\rm m} \left(\frac{H_0}{c}\right)^2 \int_0^{\chi} {\rm d}\chi' \frac{(\chi - \chi')\chi'}{\chi a(\chi')} \, \delta\left(\chi' \boldsymbol{\theta}, \chi'\right).$$

and write $D_{\rm s}$ for the distance of the source, and $D_{\rm ls}$ for the distance between lens and source. Write all distances as proper, not comoving distances, express the density contrast in terms of the density, $\delta = \Delta\rho/\bar{\rho}$, and use the critical density $\rho_{\rm crit}$.

Tangential shear and surface mass II

Assume that the lens mass distribution ρ extends over the inverval $[D_\mathrm{l} - \Delta D/2; D_\mathrm{l} + \Delta D/2]$.

$$\kappa(\boldsymbol{\theta}) = \frac{4\pi G}{c^2} \frac{D_\mathrm{l} D_\mathrm{ls}}{D_\mathrm{s}} \int_{D_\mathrm{l}-\Delta D/2}^{D_\mathrm{l}+\Delta D/2} \mathrm{d}D \, \Delta\rho(D\boldsymbol{\theta}, D).$$

Define the *critical surface mass density*

$$\Sigma_\mathrm{cr}^{-1}(\theta) := \frac{4\pi G}{c^2} \frac{D_\mathrm{l} D_\mathrm{ls}}{D_\mathrm{s}}$$

to write convergence as

$$\kappa(\boldsymbol{\theta}) = \frac{\Sigma(\boldsymbol{\theta})}{\Sigma_\mathrm{cr}}. \tag{1}$$

[Why is Σ_cr called *critical* surface mass?]
With that, we define the surface mass excess

$$\Delta\Sigma(\leq \theta) := \langle \gamma_\mathrm{t} \rangle (\theta) \, \Sigma_\mathrm{cr} = \bar{\Sigma}(\theta) - \langle \Sigma \rangle (\theta).$$

Statistical galaxy-galaxy lensing (GGL) I

The convergence or tangential shear defined in the last slides depend linearly on the mass distribution ρ, or Σ. So it seems to be a first-order statistic.

However, when measured statistically using a population of foreground galaxies, it can be written as two-point correlation function. The convergence is then the correlation of background lensing convergence and foreground galaxy position.

If we write the latter as galaxy over-density δ_g, we get

$$\begin{aligned}
\langle\kappa\rangle(\theta) &= \langle\kappa(\boldsymbol{\vartheta})\delta_\mathrm{g}(\boldsymbol{\vartheta}+\boldsymbol{\theta})\rangle_{\boldsymbol{\vartheta}} \\
&= \Sigma_\mathrm{cr}^{-1}\bar{\rho}\int \mathrm{d}D\ \langle\delta(D\boldsymbol{\theta},D)\delta_\mathrm{g}(D_\mathrm{l}\boldsymbol{\theta},D_\mathrm{l})\rangle \\
&= \Sigma_\mathrm{cr}^{-1}\bar{\rho}\int \mathrm{d}D\,\xi_{\delta\mathrm{g}}(\sqrt{(D\theta)^2+(D-D_\mathrm{l})^2}).
\end{aligned}$$

Statistical galaxy-galaxy lensing (GGL) II

Properties of statistical GGL

- Circular averages of tangential shear: robust against (some) systematic, e.g. large-scale modes of PSF residuals cancel out.
  CFHTLenS: 25% fields had to be discarded for cosmic shear, none for GGL.
- Simple null tests:
  $\langle\gamma_\times\rangle$ around foreground objects (parity mode, should vanish).
  $\langle\gamma_t\rangle$ around random points, or special points that should not be correlated with foreground sample such as chip corners, field centres, stars.
- Higher SNR compared to cosmic shear:
  correlation with tracers of dense matter regions;
  one shape instead of two;
- Can use spectroscopic galaxies for foreground sample.

Parenthesis: galaxy bias I

Simple bias

GGL measures the cross-correlation between galaxies and dark (more precisely: total) matter, $\langle \delta_{\rm g} \delta \rangle$. This correlation is non-zero since galaxies trace the underlying matter.
Simplest model: linear, constant, deterministic bias:

$$\delta_{\rm g} = b\delta.$$

From that it follws that

$$\langle \delta_{\rm g} \delta_{\rm g} \rangle(\theta) = b^2 \langle \delta\delta \rangle(\theta); \qquad \langle \delta_{\rm g} \delta \rangle(\theta) = b \langle \delta\delta \rangle(\theta),$$

or in Fourier space

$$P_{\rm gg}(k) = b^2 P_{\rm mm}(k); \qquad P_{\rm gm}(k) = b P_{\rm mm}(k).$$

Parenthesis: galaxy bias II

Properties

- The bias depends on the galaxy properties (type, color, luminosity, ...), and can be measured for different populations (e.g. early/late-type).
- Bias is redshift-dependent. Difficult to measure since degenerate with z-dependent selection effects. Volume-limited samples: Bias tends to increase with z: galaxies are more rare objects at higher z, situated in more extreme environments (halo centres).

Sample selection for galaxy bias measurement

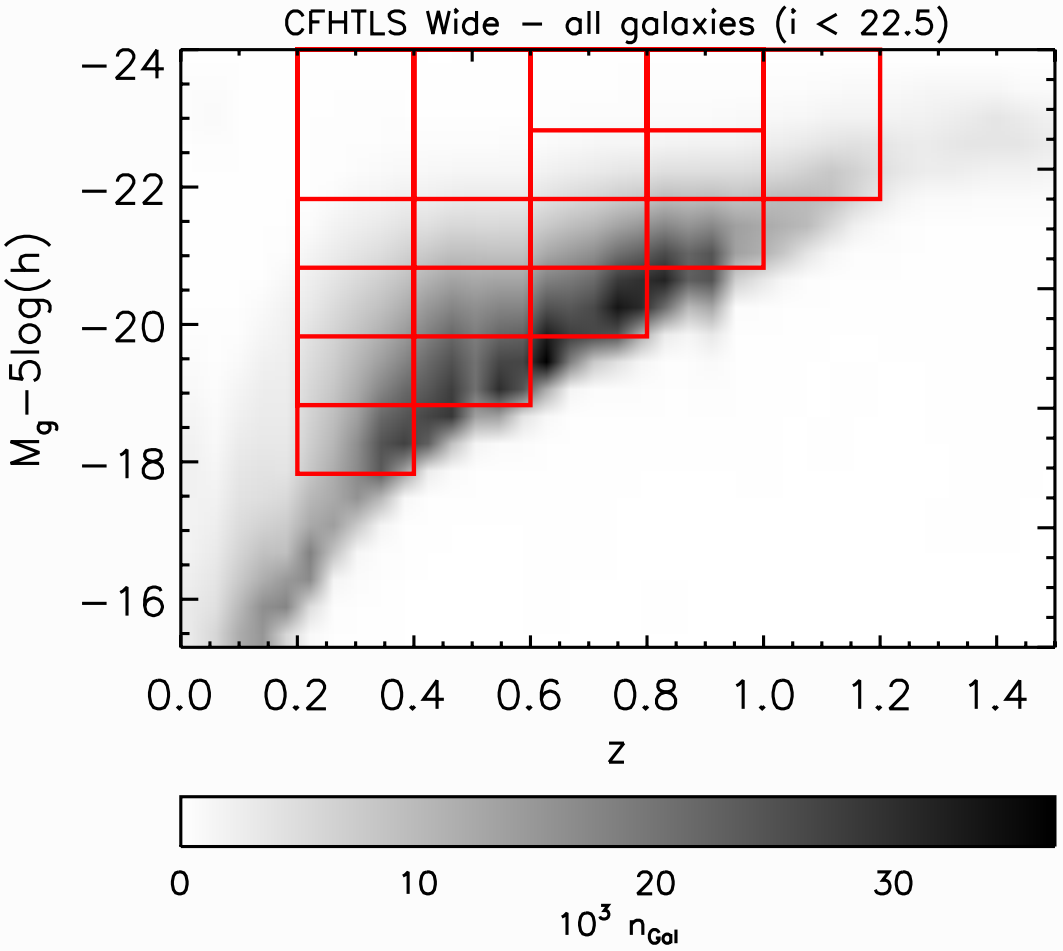

Sample selection in absolute magnitude and redshfit, from (Coupon et al. 2012).
Samples in horizontal boxes have same absolute magnitudes and are volume-limited.

Galaxy bias extended I

More complex bias models

- Scale-dependence, $b(\theta)$, or $\hat{b}(\hat{k})$. In particular on small scales, bias is not constant.
- Non-linear bias

$$\delta_{\rm g} = b_1\delta + b_2\delta^2 + b_3\delta^3 + \dots$$

- Stochastic bias

  Relation between $\delta_{\rm g}$ is not determinstic ($\delta_{\rm g} = b\delta$) but stochastic. In a statistical picture, the two fields $\delta_{\rm g}$ and δ can be interpreted as realizations of random fields with joint pdf $p(\delta_{\rm g}, \delta)$. The study of stochastic biasing is trying to quantify this joint pdf.

Galaxy bias extended II

At second-order level, one can measure the variances of both fields, and their cross-correlation. If the fields are correlated, one can write down the following two relations:

$$b = \frac{\sigma_\mathrm{g}}{\sigma} = \sqrt{\frac{\langle\delta_\mathrm{g}^2\rangle}{\langle\delta^2\rangle}}; \quad r = \frac{\sigma_\mathrm{gm}^2}{\sigma_\mathrm{g}\sigma} = \frac{\langle\delta_\mathrm{g}\delta\rangle}{\sqrt{\langle\delta_\mathrm{g}^2\rangle\langle\delta^2\rangle}}$$

introducing a correlation coffecient $r = -1 \ldots 1$ between both fields.

In the above ratio cosmology dependence (dm correlation function or power spectrum) mainly drops out!

Allows for model-independent measurement.

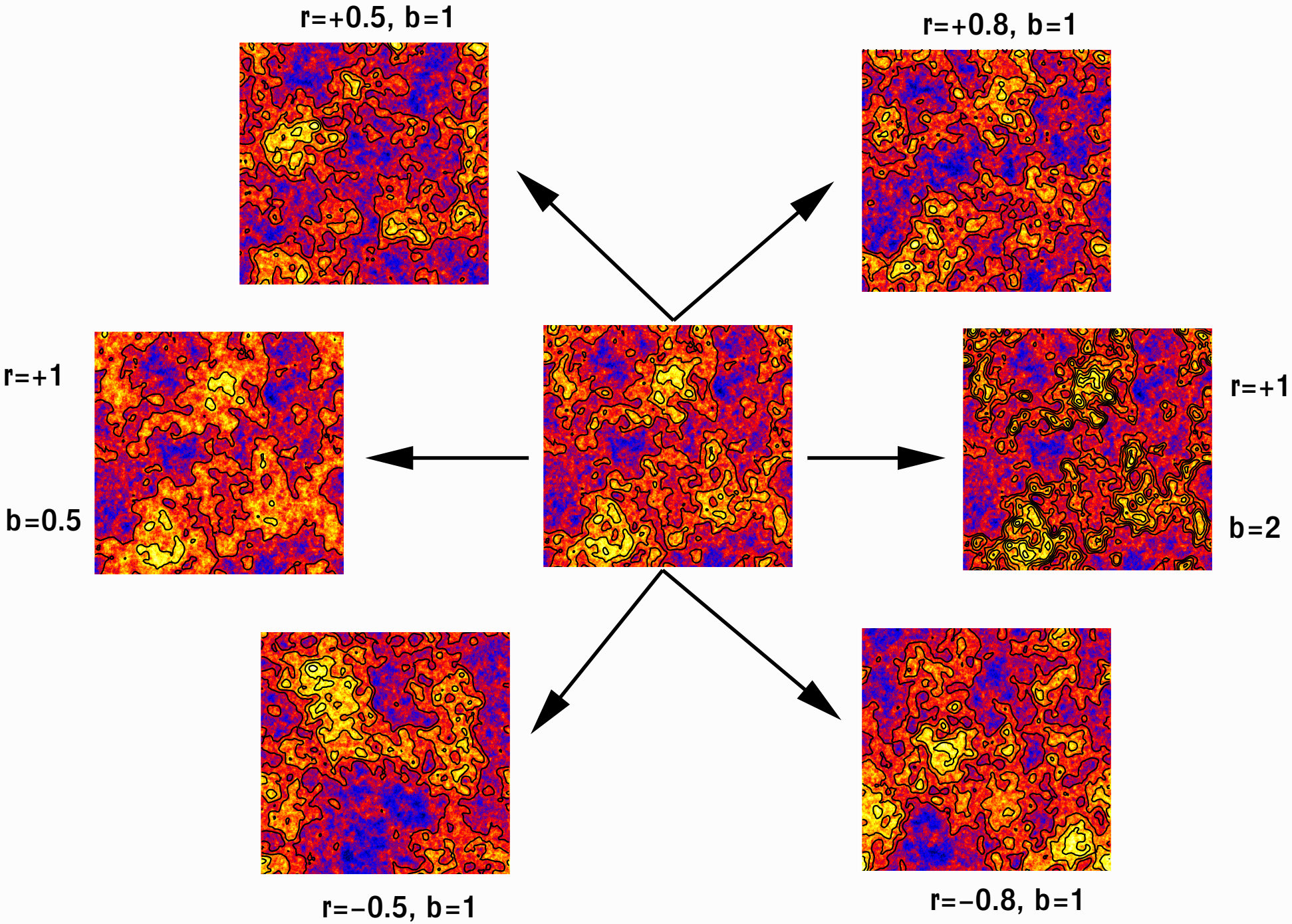

Illustration of correlated fields, from [P. Simon, PhD thesis, 2005].

Galaxy bias II

Question: How would the correlation between δ_g and δ look like for negative bias $b < 0$? For example $b = -1, r = 1$.

Non-linear and stochastic bias

A non-linear bias can mimic stochasticity.
Consider the (made-up) example of deterministic bias with $\delta_g = \delta^3$.

Exercise:

Calculate r in the case where both fields follow Gaussian pdf's.

Galaxy bias II

Question: How would the correlation between δ_g and δ look like for negative bias $b < 0$? For example $b = -1, r = 1$.

Non-linear and stochastic bias

A non-linear bias can mimic stochasticity.
Consider the (made-up) example of deterministic bias with $\delta_g = \delta^3$.
Exercise:
Calculate r in the case where both fields follow Gaussian pdf's.

$$r = \frac{\langle \delta_g \delta \rangle}{\sqrt{\langle \delta_g \delta_g \rangle \langle \delta \delta \rangle}} = \frac{\langle \delta^4 \rangle}{\sqrt{\langle \delta^6 \rangle \langle \delta^2 \rangle}} = \frac{3\sigma^4}{\sqrt{15\sigma^6\sigma^2}} = \frac{3}{\sqrt{3 \cdot 5}} = \sqrt{\frac{3}{5}} \approx 0.77 \leq 1!$$

Final note: The cosmological density field *cannot* be a Gaussian, since $\delta \leq -1$.

GGL: model-independent measurement of b/r

Idea:
Combine weak lensing and galaxy clustering to determine b and r.

- Galaxy clustering $\langle\delta_\mathrm{g}^2\rangle$
- Galaxy-galaxy lensing $\langle\delta_\mathrm{g}\delta\rangle$
- Cosmic shear $\langle\delta^2\rangle$

Cosmic shear is the most difficult to measure, so first measurements only used GC and GGL.

Form ratio:

$$\frac{\langle\delta_\mathrm{g}\delta\rangle(\theta)}{\langle\delta_\mathrm{g}\delta_\mathrm{g}\rangle(\theta)} = \frac{br}{b^2} = \frac{b}{r}.$$

Any cosmology-dependence, e.g. of clustering, drops out in the ratio.
These density correlations are projected to weak-lensing observables, and b and r (if constant) can directly be measured.

GGL: Aperture measures I

So: Combine all three

$$\langle \delta_{\rm g}^2 \rangle, \langle \delta_{\rm g} \delta \rangle, \langle \delta^2 \rangle.$$

to measure b and r.
Difficulty: Structure along all redshifts contribute to cosmic shear $\langle M_{\rm ap}^2 \rangle$, not only mass associated with foreground galaxy sample $\delta_{\rm g}$.

Solutions:

- Choose background sample such that maximum lensing efficiency coincides with foreground redshift.
- Add correction functions with minor dependency on cosmology (geometry).

Redshift calibration factors

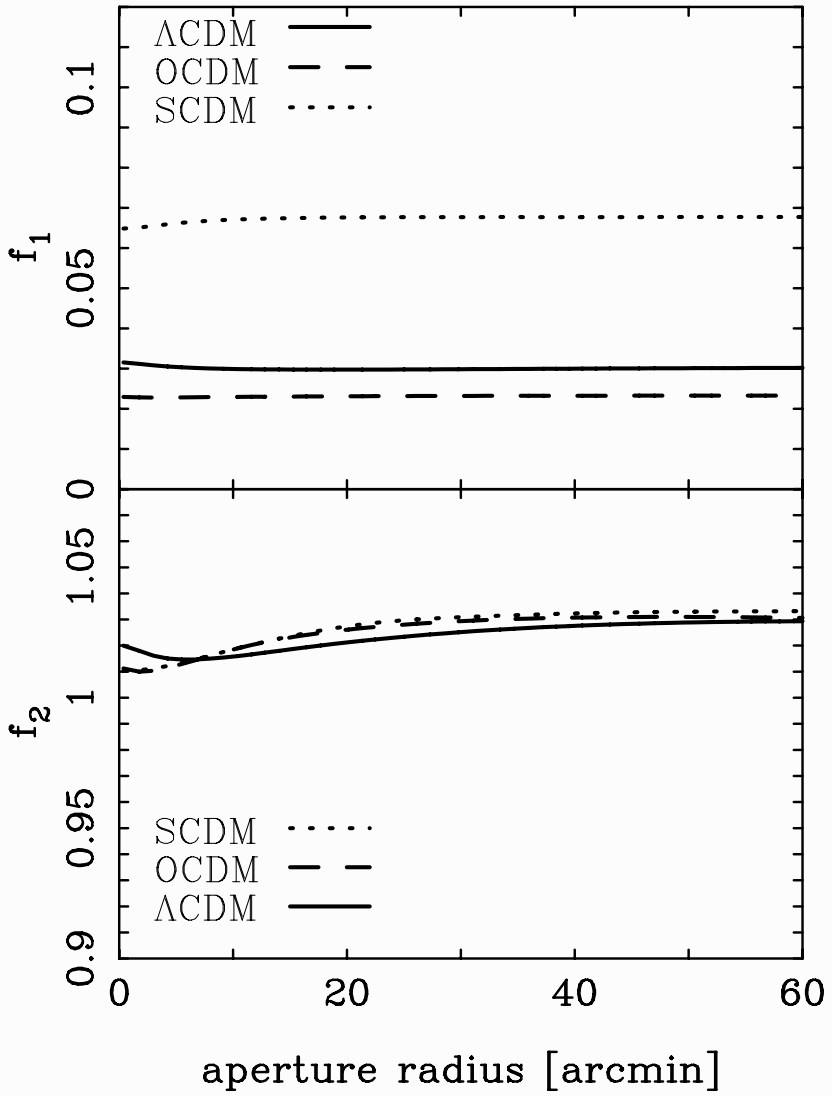

Scale-and cosmology-dependence of calibration factors. From (Simon et al. 2007), GaBoDS (Garching-Bonn Deep Survey).

GGL results: model-independent measurement of b/r

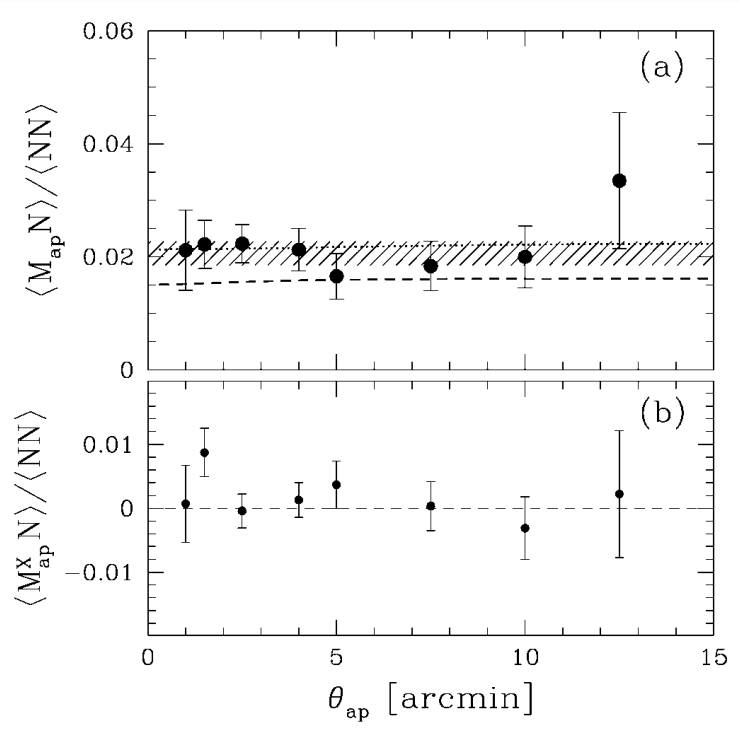

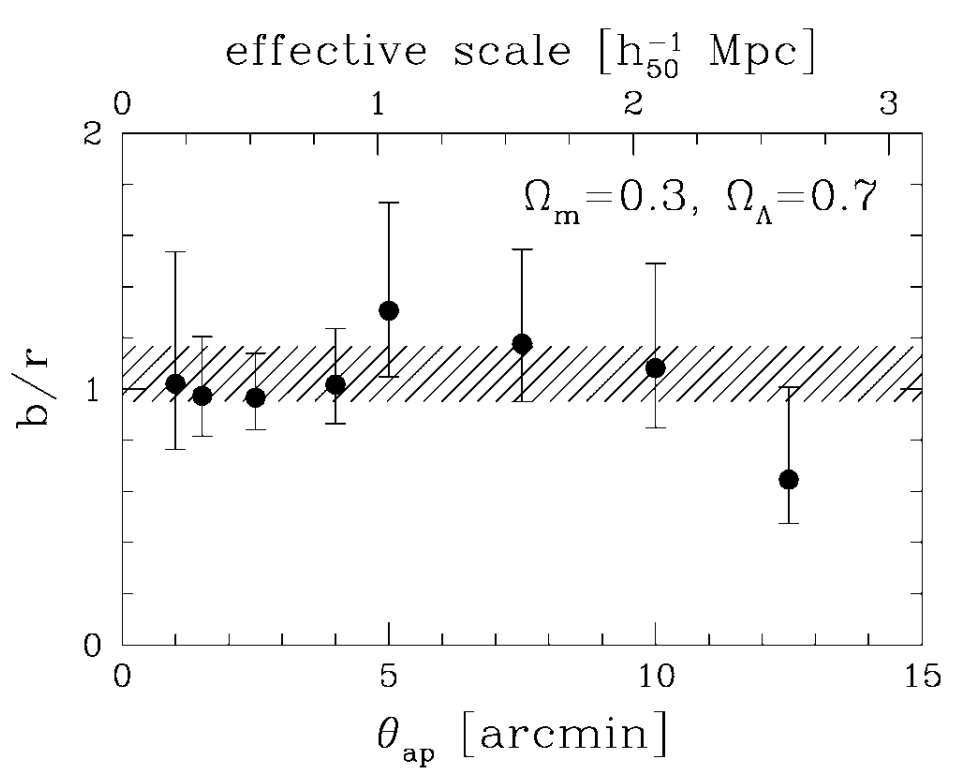

$$\mathcal{R} = \frac{r\Omega_m}{100b}[(5.8 - 1.6\Omega_m^{0.63}) + (4.6 - 2.6\Omega_m^{0.63})\Omega_\Lambda^{1.23}].$$

Observed ratio $\mathcal{R}$ (a), and B-mode (b); b/r (*right*) from (Hoekstra et al. 2001).

Main result: no scale-dependence found (on observed scales).

GGL results: model-indep. measurement of b and r I

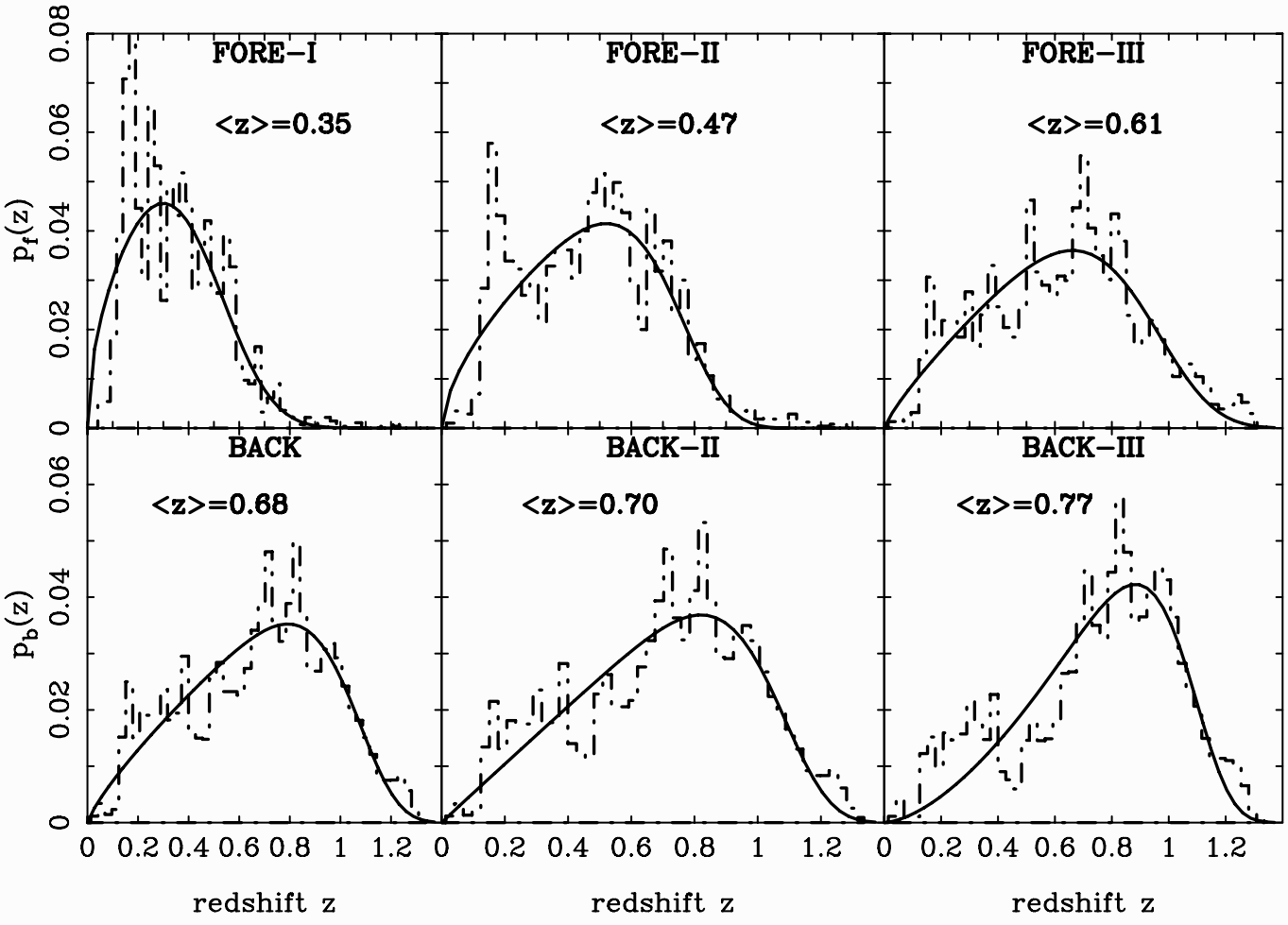

Redshift distributions for GaBoDS samples, estimated from COMBO-17. From (Simon et al. 2007), GaBoDS (Garching-Bonn Deep Survey).

GGL results: model-indep. measurement of b and r II

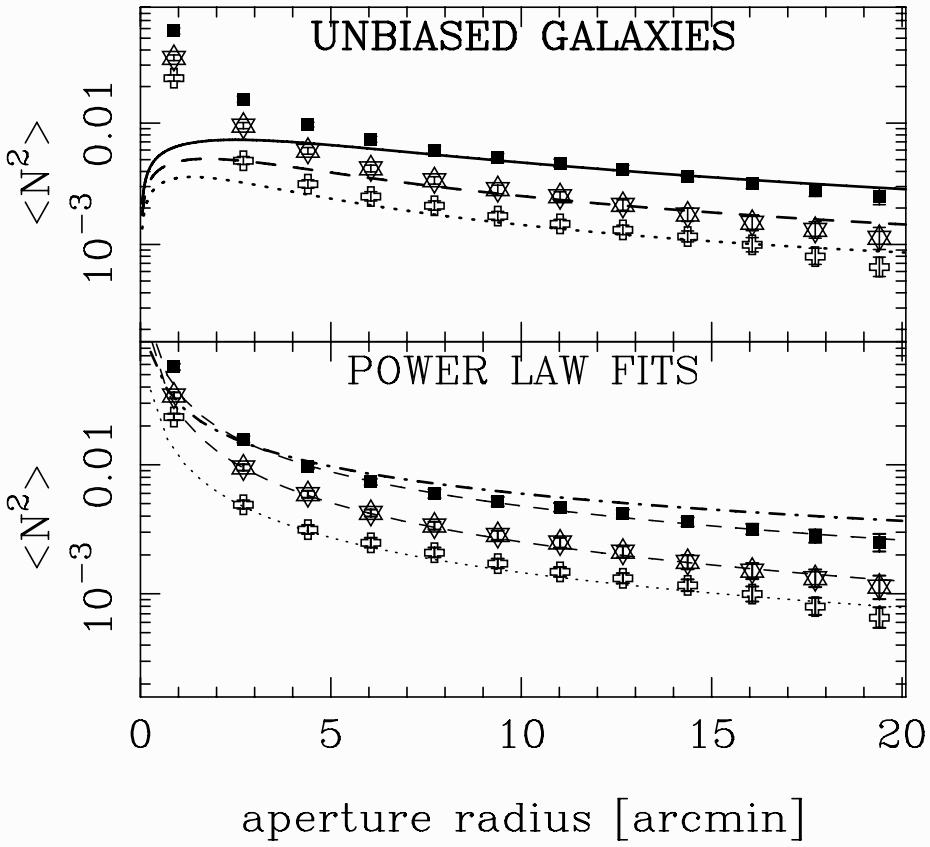

Filled boxes, open stars, open crosses = FORE-I, FORE-II, FORE-III.

Galaxy clustering: Bias on small scales is not constant, but scale-dependent. Stronger galaxy clustering than from constant bias. (Simon et al. 2007), GaBoDS (Garching-Bonn Deep Survey).

GGL results: model-indep. measurement of b and r III

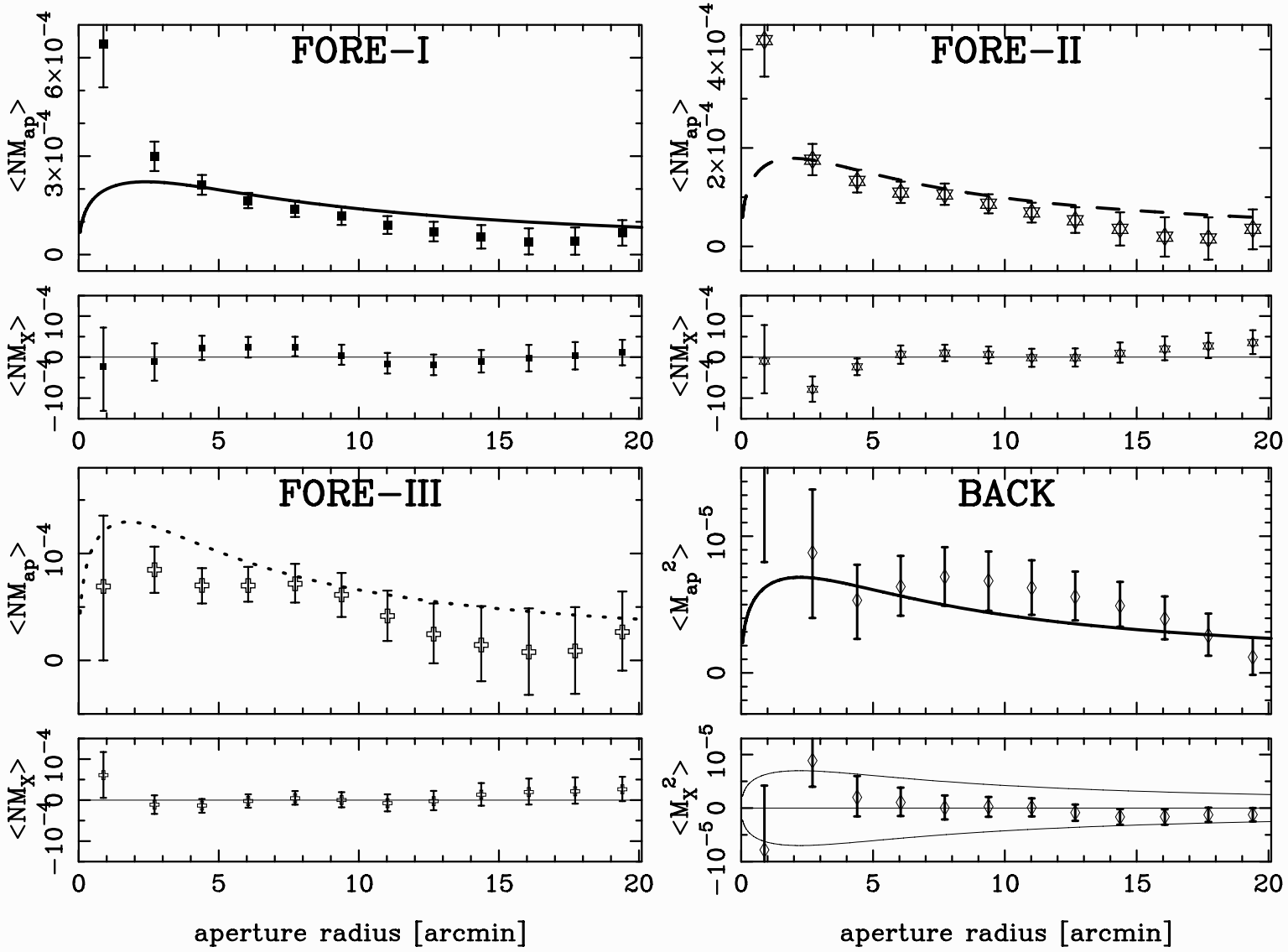

GGL and cosmic shear. (Simon et al. 2007), GaBoDS (Garching-Bonn Deep Survey).

GGL results: model-indep. measurement of b and r IV

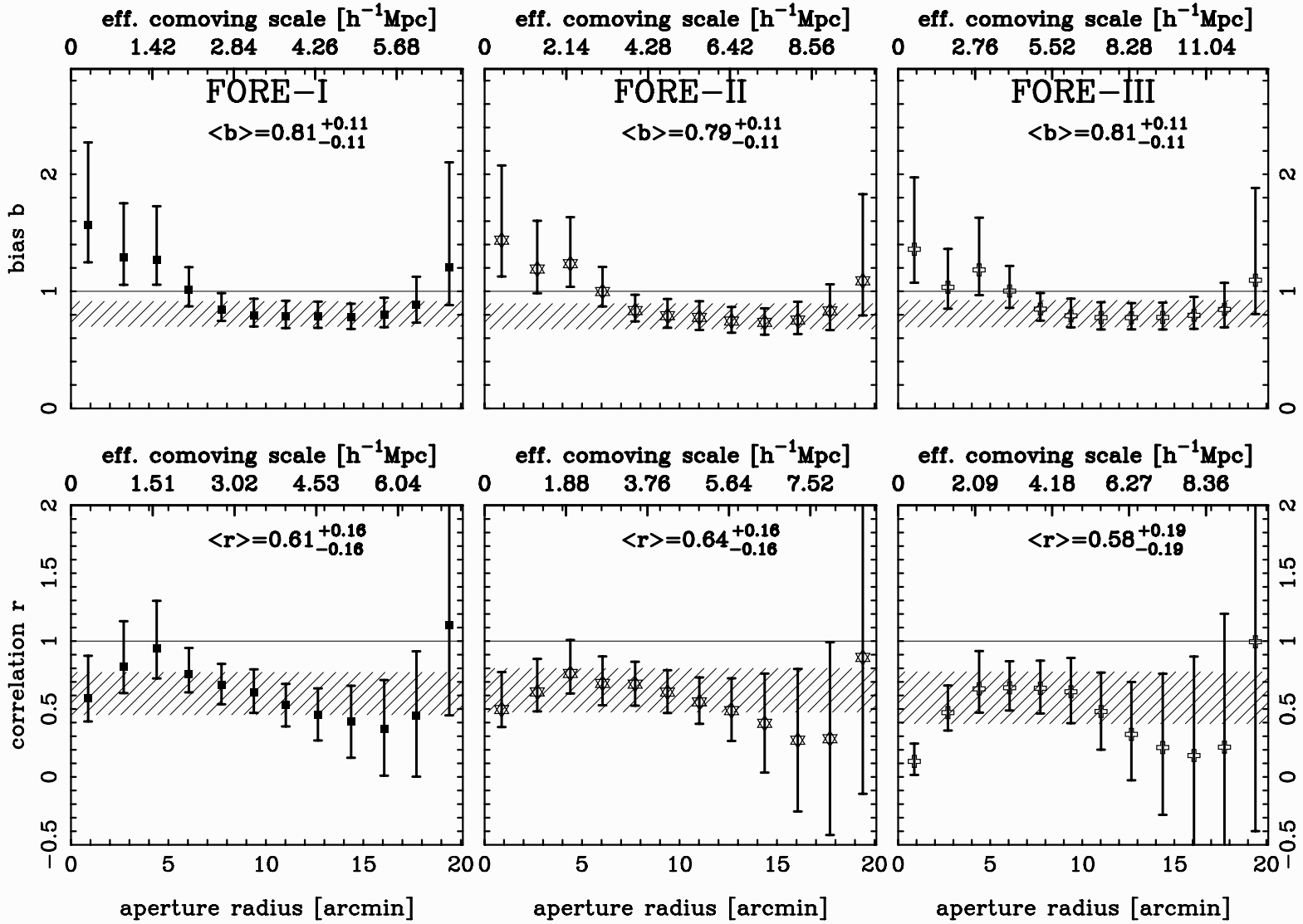

Bias and correlation coefficient. (Simon et al. 2007), GaBoDS (Garching-Bonn Deep Survey).

GGL: HOD model measurements

increasing luminosity →

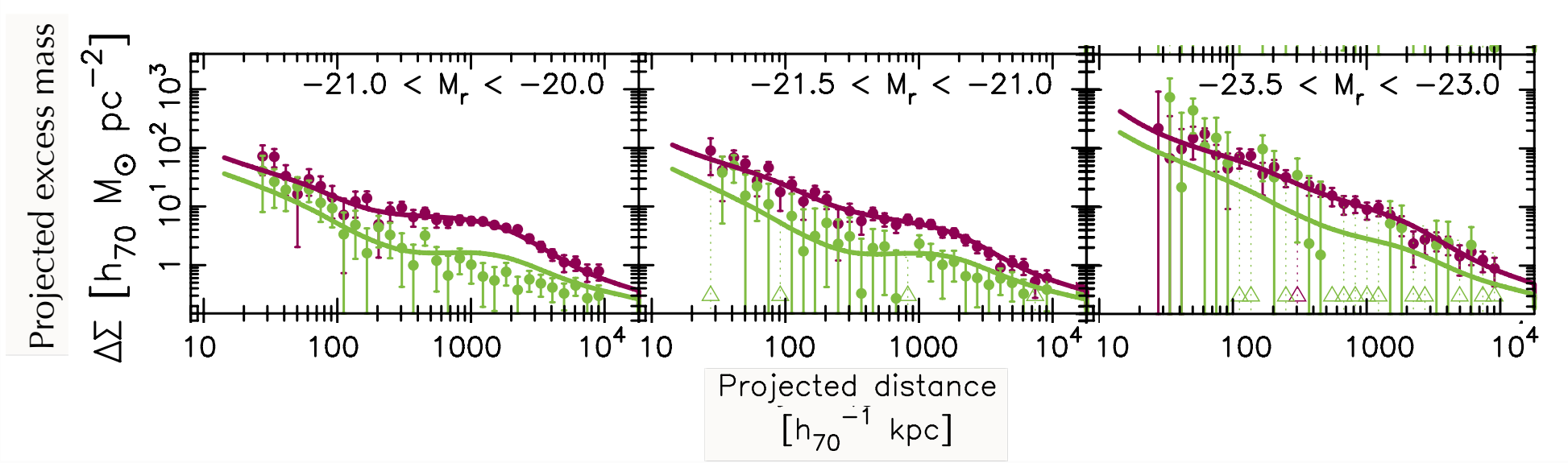

Purple=red early-type galaxies; Green=blue late-type galaxies. From (Velander et al. 2014).

GGL: HOD model measurements

increasing luminosity →

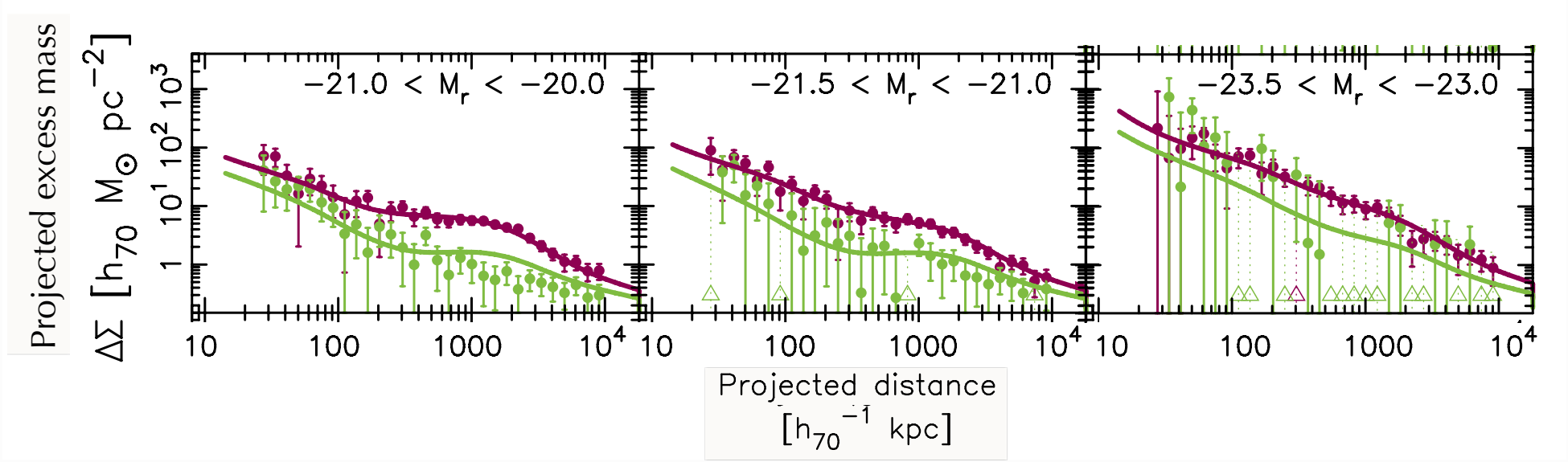

Purple=red early-type galaxies; Green=blue late-type galaxies. From (Velander et al. 2014).

- Red galaxies have larger associated mass than blue galaxies.
- Exceess mass increases with luminosity. Light traces mass.

GGL: HOD model measurements

increasing luminosity →

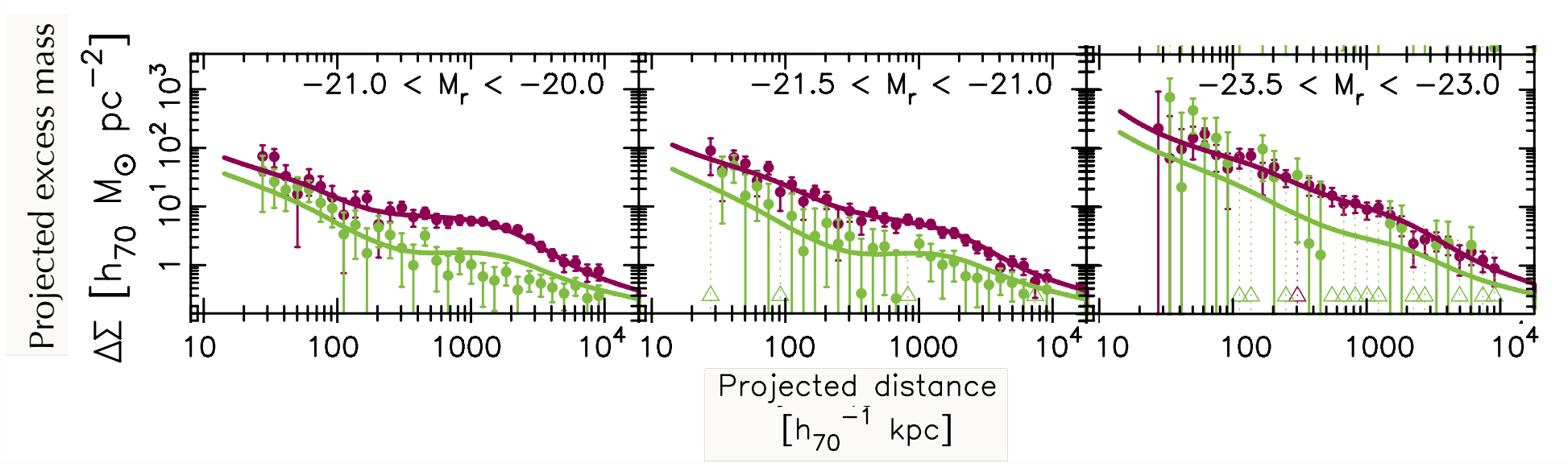

Purple=red early-type galaxies; Green=blue late-type galaxies. From (Velander et al. 2014).

- Red galaxies have larger associated mass than blue galaxies.
- Exceess mass increases with luminosity. Light traces mass.
- Bump at 1 Mpc for low-luminosity red galaxies, disappears at higher L. Red satellite galaxies.

GGL: HOD model measurements

increasing luminosity →

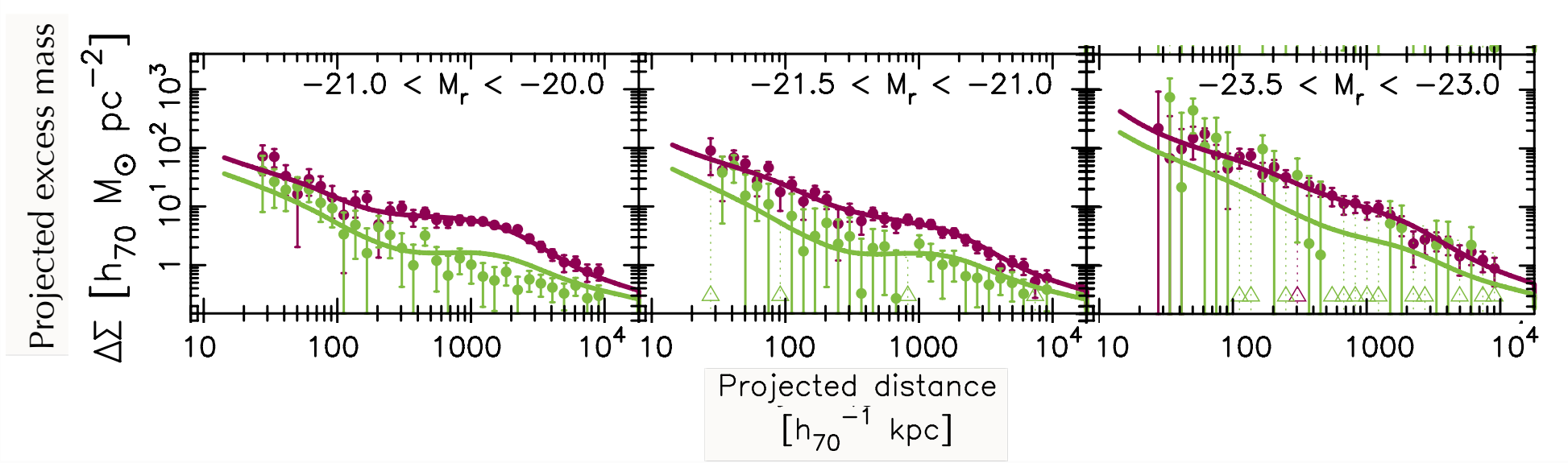

Purple=red early-type galaxies; Green=blue late-type galaxies. From (Velander et al. 2014).

- Red galaxies have larger associated mass than blue galaxies.
- Exceess mass increases with luminosity. Light traces mass.
- Bump at 1 Mpc for low-luminosity red galaxies, disappears at higher L. Red satellite galaxies.
- Bump at slightly larger scale for blue galaxies. 2-halo term, from clustered nearby galaxies.

GGL: HOD model

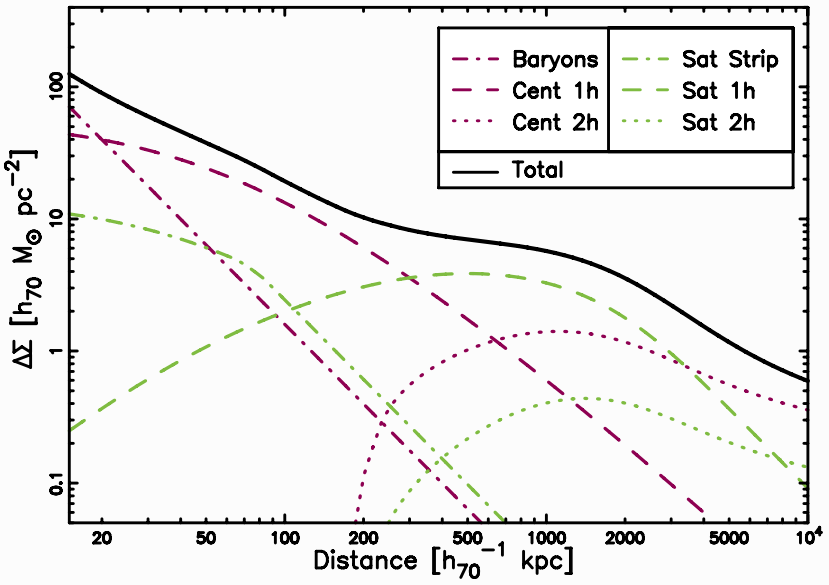

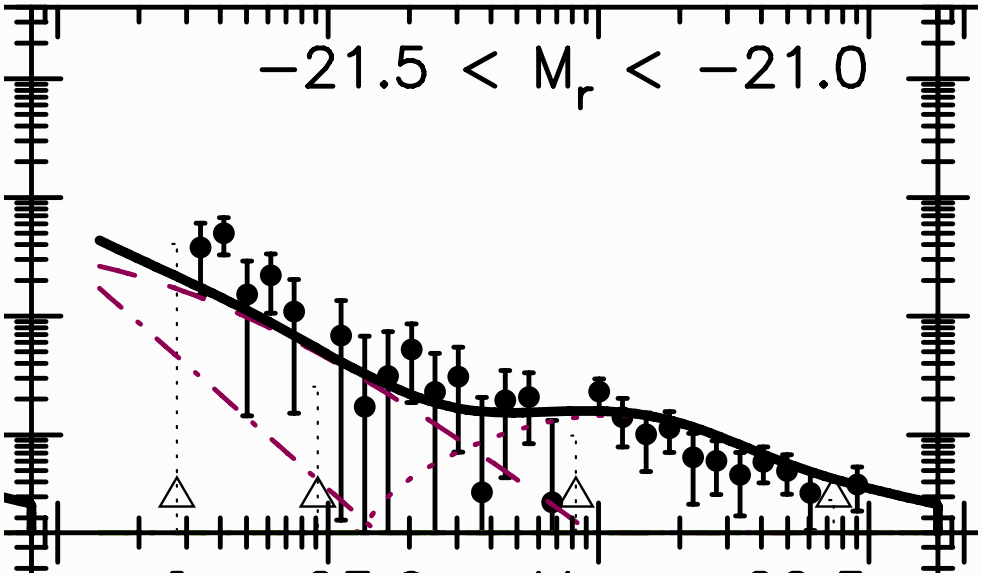

HOD model, (Velander et al. 2014).

GGL: M/L parameters

$$M_{200} = M_{0,L} \left(\frac{L}{L_{\rm fid}} \right)^{\beta_L}$$

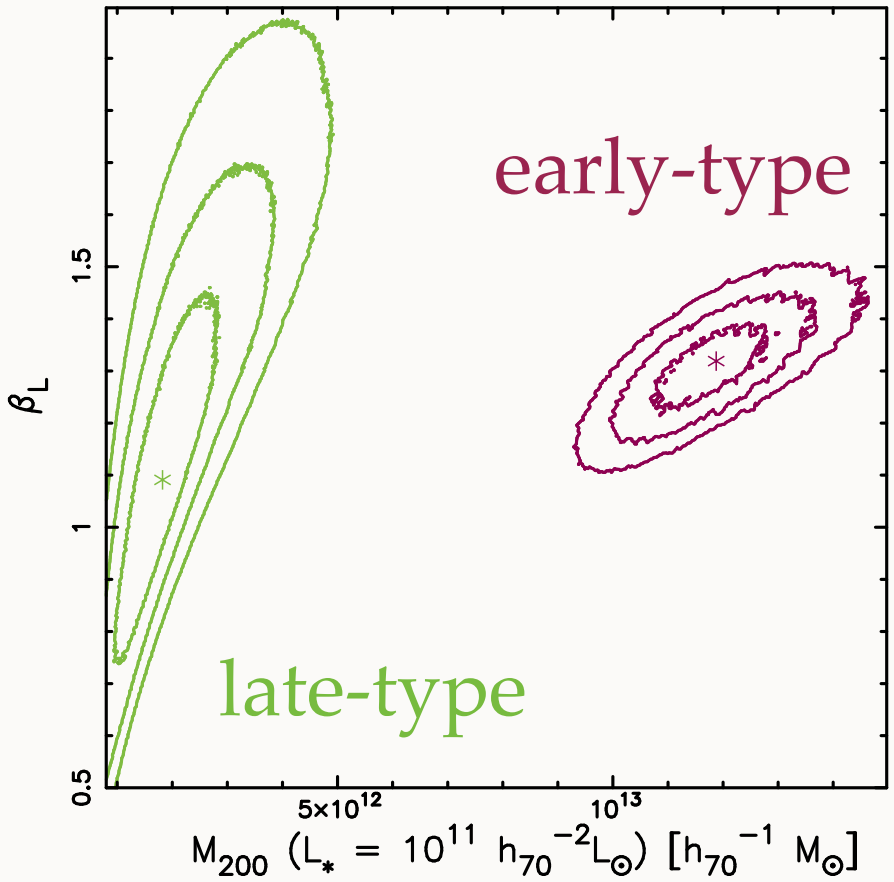

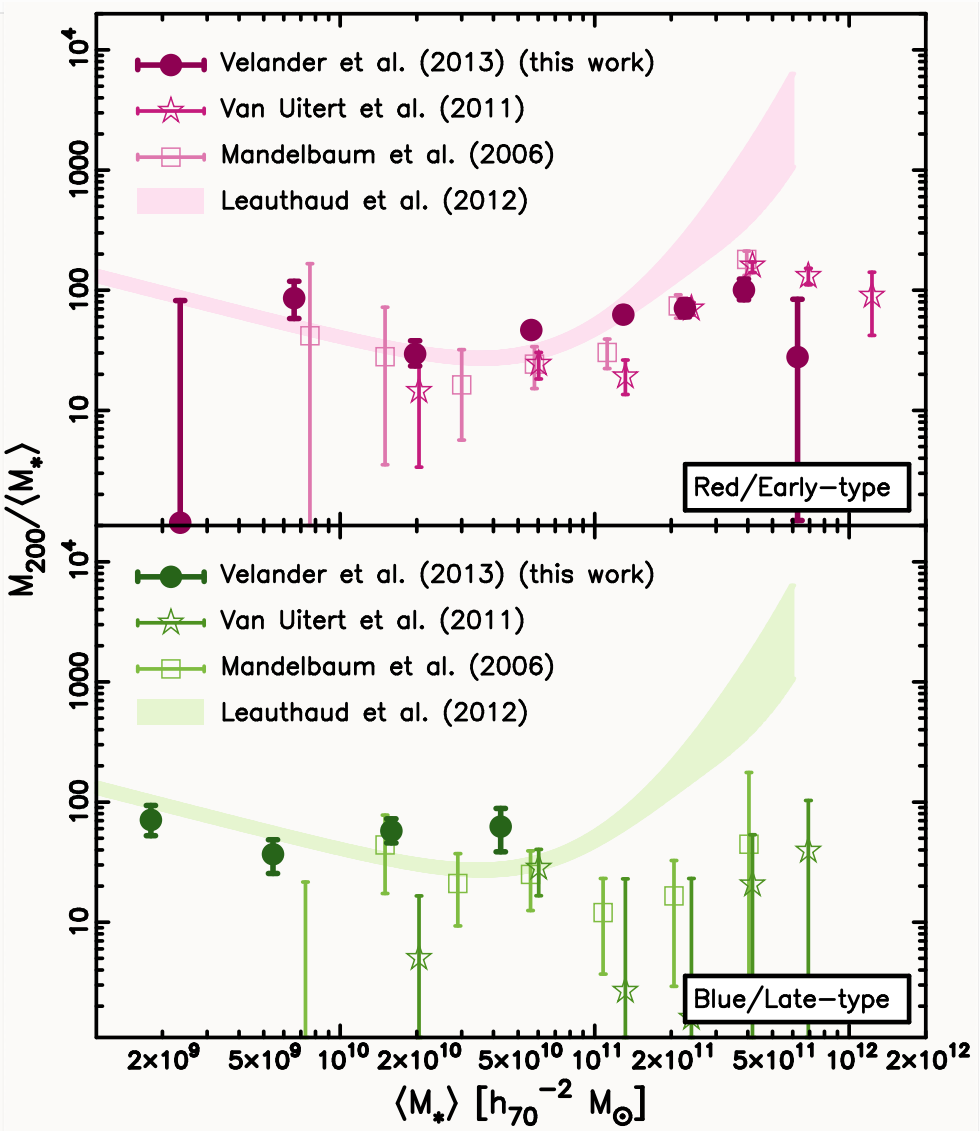

(Velander et al. 2014).